



**HAL**  
open science

## A new macroscopic model including membrane exchange for diffusion MRI

Julien Coatléven, Housseem Haddar, Jing-Rebecca Li

► **To cite this version:**

Julien Coatléven, Housseem Haddar, Jing-Rebecca Li. A new macroscopic model including membrane exchange for diffusion MRI. 2013. hal-00768732v2

**HAL Id: hal-00768732**

**<https://inria.hal.science/hal-00768732v2>**

Preprint submitted on 25 Jan 2013 (v2), last revised 25 Jan 2014 (v4)

**HAL** is a multi-disciplinary open access archive for the deposit and dissemination of scientific research documents, whether they are published or not. The documents may come from teaching and research institutions in France or abroad, or from public or private research centers.

L'archive ouverte pluridisciplinaire **HAL**, est destinée au dépôt et à la diffusion de documents scientifiques de niveau recherche, publiés ou non, émanant des établissements d'enseignement et de recherche français ou étrangers, des laboratoires publics ou privés.

# A NEW MACROSCOPIC MODEL INCLUDING MEMBRANE EXCHANGE FOR DIFFUSION MRI

J. Coatléven, H. Haddard, J-R. Li

## Abstract

Diffusion Magnetic Resonance Imaging (dMRI) is a promising tool to obtain useful information on microscopic structure and has been extensively applied to biological tissues. We establish a new macroscopic model from homogenization theory to obtain the aggregate dMRI signal measured in practice in the case of intermediate water exchange across cellular membranes. Based on a particular scaling of the permeability condition modeling cellular membranes, this model accurately reproduces the memory effects observed in practice. Explicit formulae given by homogenization for the coefficients of this model emphasize their link to the relevant physiological quantities, and the inverse problem of retrieving these coefficients from a set of measurements is considered.

## 1 INTRODUCTION

Diffusion MRI can be interpreted as a measurement of the diffusion of water molecules in tissues, and thus any modification in this measure could provide useful information on changes in the biological tissue[15], such as cell swelling[1, 4, 11, 12, 24], demyelinating disorders[13], neuronal activity[9, 16] or the presence of tumors [19, 21, 23]. The potential clinical applications of diffusion MRI have thus multiplied during the last 25 years, making it a promising diagnosis tool in many diseases. However, the link between the physiological parameters and the measured signal has mostly remained only qualitatively explained. This is why we aim here at providing a mathematical model that reproduces accurately the link between the dMRI signal and the average properties of the probed biological tissue.

More precisely, we aim at providing an accurate model for the signal typically obtained with clinical MRI scanners. This signal is a mean value of water magnetization on a domain (the imaging voxel) whose size is much greater than the size of the biological cells. Thus, the signal is a macroscopic quantity with respect to the underlying tissue. For this reason, starting from the complete description of the diffusion phenomenon at the microscopic level, which mathematically takes the form of a Bloch-Torrey PDE in a heterogeneous medium with barriers, varying at the scale of biological cells, we will provide a macroscopic limit model, through homogenization. The signal associated to this macroscopic (and homogeneous) model, being in principle the limit when the size of biological cells tends to zero of the real signal, is thus expected to be a very accurate approximation of the non-homogenized one at long diffusion times. The equations governing this signal will be of course much simpler than those involving the microscopic description of the medium. Their coefficients can be explicitly linked, in the context of periodic homogenization, to relevant properties of the underlying biological tissue. The inverse problem of identifying the coefficients that makes our approximate signal fit best the measured signal will be a much more tractable problem than original inverse problem based on the Bloch-Torrey PDE on a heterogeneous domain.

The paper will be organized as follows. In the first section, we recall the Bloch-Torrey PDE with barriers that accurately describes the dynamics involved in dMRI experiments at the microscopic level. For simplicity, we then make the hypothesis that the medium is periodic, to allow us to apply periodic homogenization theory. The reason for doing so is that it is well known that even for media

that are not truly periodic, the homogenized limit obtained in the periodic case remains formally accurate for describing the generic case (see for instance [2] and [3] for the case of porous media), i.e. the macroscopic equations remains of the same analytical form in every case (only the exact values of the coefficients change). In a second section, we make the formal homogenization of our model problem in the periodic context, using a particular scaling for the permeability conditions modeling cellular membranes. In the next section, we provide an ODE description of the measured signal when the domain is unbounded. We then show with a few numerical experiments that this model for the homogenized signal accurately fits the signal obtained without homogenization. Finally, we solve numerically the inverse problem of finding the coefficients of our ODE model from the signal obtained without homogenization, and show that through these coefficients we accurately recovers some relevant biological properties of the tissue.

## 2 MODEL PROBLEM

A classic dMRI experiment consists of applying two pulsed (meaning short duration in time) gradient (meaning linearly varying in space) magnetic fields with a 180 degree spin reversal in between the two in order to mark the positions of the water molecules between the two pulses. Water molecules exist in abundance in biological tissues, hence the interest in measuring water displacement to probe tissue microstructure.

Biological tissues are mainly composed of cells of various sizes and shapes surrounded by extra-cellular fluid. The cells can be represented, at the scale of interest for our problem, as a bounded domain surrounded by a very thin membrane (see Figure 1). The diffusion coefficients for water in

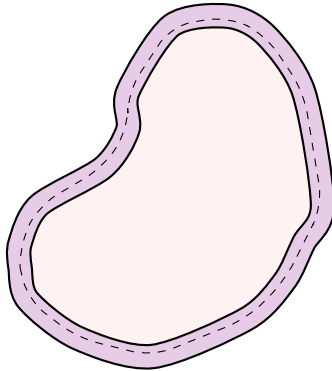


Figure 1: Schematic of a biological cell, with its membrane

the interior part of the cell, in the membrane, and in the surrounding fluid, may be different from each other.

While the diffusion coefficients in the interior part of the cell and in the surrounding fluid remain of the same order of magnitude, it is much smaller inside the membrane. It is in fact extremely difficult to obtain direct measurements of this coefficient inside the cellular membrane, as this membrane is extremely thin. This is why the membrane is most of the time spatially neglected and replaced by a permeability condition between the extra-cellular and intra-cellular parts [18]. Consequently, we can say that we replace the realistic, "three-compartment" biological cell by the "two-compartment" cell displayed in Figure 2. For an imaging voxel  $\Omega$  of biological tissue, we denote by  $\Gamma_{\mathcal{I}}$  the union of the boundaries of all the "two-compartment" cells included in  $\Omega$ .  $\Gamma_{\mathcal{I}}$  thus delimits two subdomains : the extracellular domain  $\Omega_e$  ( $e$  standing for extra-cellular) and the intra-cellular domain  $\Omega_c$  ( $c$  standing for cellular) . The domain  $\Omega_{ext}$  then represents the union of the open extra-cellular and

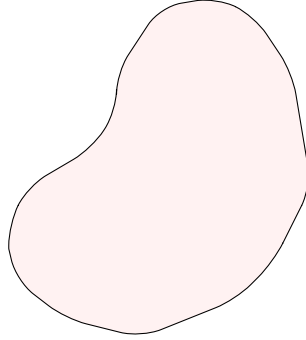


Figure 2: A simplified, two-compartment cell

open intra-cellular domains, i.e. :

$$\Omega_{ext} = \Omega \setminus \Gamma_{\mathcal{I}} = \Omega_e \cup \Omega_c$$

The water magnetization  $M$  is modeled by the following Bloch-Torrey PDE [22] with jump :

$$\begin{aligned} \frac{\partial M(\mathbf{x}, t)}{\partial t} + \imath \mathbf{q} \cdot \mathbf{x} f(t) M(\mathbf{x}, t) - \text{div}(\sigma(x) \nabla M(\mathbf{x}, t)) &= 0 && \text{in } \Omega_{ext} \times ]0, T[ \\ \sigma \nabla M \cdot \nu|_{\Gamma_{\mathcal{I}}} &= \kappa [M]_{\Gamma_{\mathcal{I}}} && \text{on } \Gamma_{\mathcal{I}} \\ [\sigma \nabla M \cdot \nu]_{\Gamma_{\mathcal{I}}} &= 0 && \text{on } \Gamma_{\mathcal{I}} \\ M(\cdot, 0) &= M_{init} && \text{in } \Omega_{ext} \end{aligned}$$

where  $\nu$  is the normal exterior to the intra-cellular domains,  $[\cdot]_{\Gamma_{\mathcal{I}}}$  is the jump (extra-cellular minus intra-cellular) on  $\Gamma_{\mathcal{I}}$  for a quantity defined on both parts of the domain,  $\kappa$  is the permeability coefficient,  $\imath = \sqrt{-1}$ ,  $M_{init}$  is the initial magnetization. The constant vector in  $\mathbb{R}^d$ ,  $\mathbf{q}$ , contains the amplitude and direction of the applied magnetic field and the gyro-magnetic ratio of the water proton, and  $f$ , where  $\max_t f(t) = 1$ , is the normalized time profile of the diffusion-encoding magnetic field. The coefficient  $\sigma$  is the diffusion coefficient for water. The time profile of the classic Pulsed Gradient Spin Echo (PGSE) [20] sequence is the following:

$$\begin{cases} f(t) = 0, & t \leq 0; \\ f(t) = 1, & 0 < t \leq \delta; \\ f(t) = 0, & \delta < t \leq \Delta; \\ f(t) = -1, & \Delta < t \leq \Delta + \delta; \\ f(t) = 0, & \Delta + \delta < t; \end{cases}$$

where we made  $f(t)$  negative in the second pulse to include the effect of the 180 degree spin reversal between the pulses. The pulse duration  $\delta$  can be anywhere from two to tens of milliseconds. The duration between pulses,  $\Delta$ , can be from tens to a hundred milliseconds, depending on tissue type. The time at which the signal is measured is called the echo time and it is  $TE = \delta + \Delta$ .

In general, the imaging voxel would have a side length of at least a millimeter, whereas the diameter of the cells in the brain would be on the order of micrometers. Hence, there would be at least tens of thousands of cells in an imaging voxel, justifying our approach that treats the many cells in an aggregate or homogenized way.

For simplicity and in order to be able to apply a well known theoretical framework, we will assume that the imaging voxel  $\Omega$  can be described as a periodic domain. More precisely, we will

assume that there exists a period  $\varepsilon$ , which represents the average size of a "representative" volume of the imaging voxel, and will be assumed to be small compared to the size of  $\Omega$ . In practice, this  $\varepsilon$  will be taken to be between 10 and 50 micrometers.

We now define the unit periodicity cell  $Y = ]0, 1[^d$  such that:

$$Y = Y_e \cup Y_c$$

where  $Y_c$  is the intracellular domain, and is an open set which can be made of several connected parts (i.e it is the union of the interiors of the selection of biological cells that are included in the periodicity cell). Let  $N_c$  be the number of connected components of  $Y_c$ . We write :

$$Y_c = \bigcup_{i=1}^{N_c} Y_{c,i}$$

Then, we define  $Y_e = Y \setminus \overline{Y_c}$ , the extracellular domain. In the same way, we write :

$$Y_e = \bigcup_{i=1}^{N_e} Y_{e,i}$$

where  $N_e$  is the number of connected components of  $Y_e$ . If some cells touch each other and isolate a part of  $Y_e$ , then  $N_e \neq 1$ . We assume for simplicity that the boundary  $\partial Y_c$  of  $Y_c$  does not crosses  $\partial Y$  and we denote it  $\Gamma_m = \partial Y_c = \partial Y_e \setminus \overline{\partial Y}$ . The general case can be treated in exactly the same way, but the geometrical description is more complicated : indeed, if  $\Gamma_m$  crosses  $\partial Y$ , then the biological cell must be periodically closed by another component of  $Y_c$  on the opposite side of  $\partial Y$ , so that the periodicized domain only contains biological cells completely surrounded by membranes.

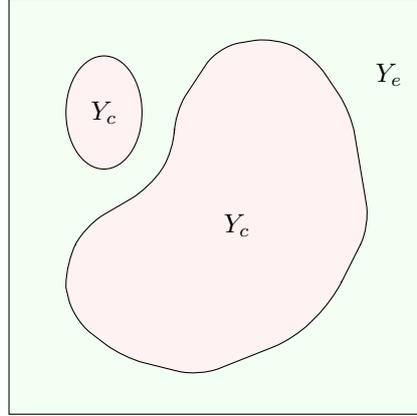


Figure 3: A periodic cell  $Y$ , containing simplified biological cells with an infinitely thin interface for membrane

Now, we denote :

$$\Xi_\varepsilon = \{\xi \in \mathbb{Z}^d \mid \varepsilon(\xi + Y) \cap \Omega \neq \emptyset\}$$

so that  $\Omega$  will contain almost  $\sharp(\Xi_\varepsilon)$  periodic cells. Finally, we denote :

$$\left\{ \begin{array}{l} \overline{\Omega}_e^\varepsilon = \bigcup_{\xi \in \Xi_\varepsilon} \varepsilon(\xi + \overline{Y_e}) \cap \overline{\Omega} \\ \Omega_c^\varepsilon = \bigcup_{\xi \in \Xi_\varepsilon} \varepsilon(\xi + Y_c) \cap \Omega \\ \Omega_{ext}^\varepsilon = \Omega_e^\varepsilon \cup \Omega_c^\varepsilon \end{array} \right. \quad (1)$$

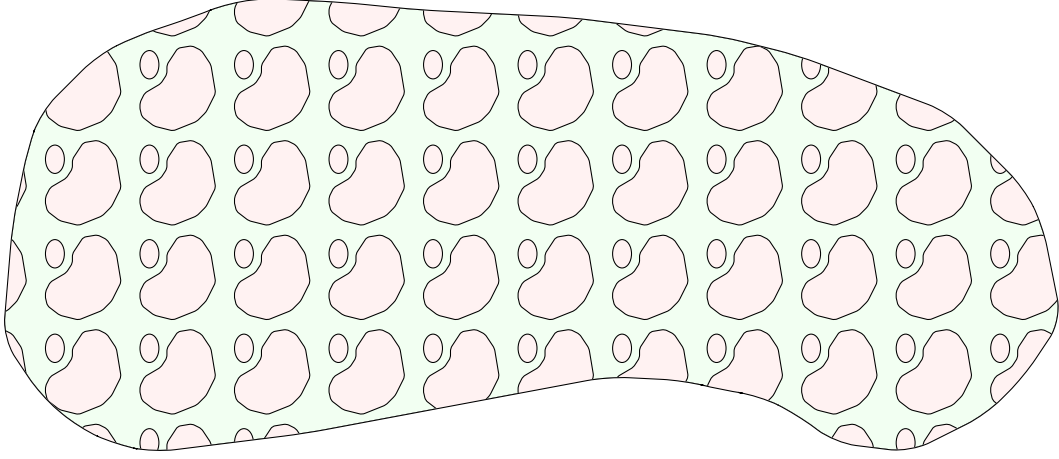


Figure 4: The periodic  $\Omega_{ext}^\varepsilon$

Notice that :

$$\partial\Omega_c^\varepsilon \cap \partial\Omega_e^\varepsilon = \partial\Omega_e^\varepsilon \setminus \overline{\partial\Omega} = \bigcup_{\xi \in \Xi_\varepsilon} \Gamma_m^{\varepsilon, \xi} \quad \text{where} \quad \Gamma_m^{\varepsilon, \xi} = \varepsilon(\xi + \Gamma_m) \cap \Omega$$

Of course, the diffusion coefficient will be assumed to be periodic as well, i.e there exists  $\hat{\sigma} \in L^\infty(Y)$  such that  $\sigma(x) = \hat{\sigma}(\frac{x}{\varepsilon})$ , with :

$$\hat{\sigma} = \begin{cases} \sigma_c & \text{in } Y_c \\ \sigma_e & \text{in } Y_e \end{cases} \quad (2)$$

The most common practical choice for  $\sigma_e$  and  $\sigma_c$  is to take them constant, so that  $\hat{\sigma}$  is piecewise constant. For both physical and technical reasons, we will further assume that there exists two constants  $0 < \sigma^- < \sigma^+ < +\infty$  such that, for almost every  $y \in Y$

$$\sigma^- \leq \sigma_c \leq \sigma^+ \quad \text{and} \quad \sigma^- \leq \sigma_e \leq \sigma^+$$

With these more precise description of the domain, our model problem can be rewritten :

$$\boxed{\begin{aligned} \frac{\partial M_\varepsilon(\mathbf{x}, t)}{\partial t} + \nu \mathbf{q} \cdot \mathbf{x} f(t) M_\varepsilon(\mathbf{x}, t) - \operatorname{div}(\hat{\sigma}_\varepsilon(x) \nabla M_\varepsilon(\mathbf{x}, t)) &= 0 & \text{in } \Omega_{ext}^\varepsilon \times ]0, T[ \\ \hat{\sigma}_\varepsilon \nabla M_\varepsilon \cdot \nu|_{\Gamma_m^{\varepsilon, \xi}} &= \kappa^\varepsilon [M_\varepsilon]|_{\Gamma_m^{\varepsilon, \xi}} & \forall \xi \in \Xi_\varepsilon \\ [\hat{\sigma}_\varepsilon \nabla M_\varepsilon \cdot \nu]|_{\Gamma_m^{\varepsilon, \xi}} &= 0 & \forall \xi \in \Xi_\varepsilon \\ M_\varepsilon(\cdot, 0) &= M_{init} & \text{in } \Omega_{ext}^\varepsilon \end{aligned}} \quad (3)$$

where  $\hat{\sigma}_\varepsilon = \hat{\sigma}(\frac{x}{\varepsilon})$ . Finally, we will assume that the time profile  $f$  belongs to  $L^\infty(]0, T[)$  and that the initial data  $M_{init}$  is defined on  $\Omega$  independently of  $\varepsilon$  and belongs to  $L^2(\Omega) \cap L^1(\Omega)$ .

It only remains to choose the domain  $\Omega$  itself. We want to model an "imaging voxel", i.e. the spatial domain, which is a subpart of the whole probed sample (the whole brain, for example). However, because the magnetic fields are applied to the entire probed sample, thus, two imaging voxels that have a common boundary will exchange water during the experiment. But the influence of this exchange will be small because the aggregate diffusion coefficient of water in biological tissue is at most  $10^{-3}mm^2/s$ , meaning in the longest typical diffusion time of  $\Delta = 100ms$ , the diffusion distance will be  $25\mu m$ , much smaller than the length across a voxel, which is at least  $1mm$ . Hence, a very small percentage of the water molecules in the imaging voxel come from a neighboring voxel or have left for a neighboring voxel during the echo time  $TE = \delta + \Delta$ , thus their influence and the average magnetization over the voxel can be neglected.

From the mathematical point of view, using the linearity of the equation as well as its parabolic nature, we can say that an initial condition supported in a given voxel will give birth to a contribution that will be exponentially decaying in the space outside the voxel. Thus, the measured signal in a voxel is only minorly influenced by the surrounding voxels and not at all by voxels further away. Hence we are allowed to extend our imaging voxel by periodic copies of itself instead of its actual neighboring voxels. Thus, it is reasonable to consider as a good approximation that we can pose our problem by extending the imaging voxel of interest to  $\Omega = \mathbb{R}^d$  which contains infinitely many periodic copies of the imaging voxel of interest. Given that the spatial variations between neighboring voxels are not too big in biological imaging applications, we believe that this periodic extension of the imaging voxel of interest to all of  $\mathbb{R}^d$  is a reasonable approximation.

Consequently, this is the simplified model we will explore in the following. Notice that the homogenized limit we are going to obtain would have been the same if we had considered a bounded domain with Neumann or Dirichlet boundary conditions (with the modification that the boundary conditions would then apply also to the homogenized limit).

Finally, we conclude this section by explaining our choice for the permeability coefficient  $\kappa^\varepsilon$ . As usual in homogenization, the choice of a scaling for this coefficient, driven by the fact that it is experimentally a very small parameter, will be determinant with regard to the limit model. More precisely, the behavior of  $\kappa^\varepsilon$  when  $\varepsilon \rightarrow 0$  will completely determine the limit macroscopic model. In practice, to get all the possible limit models, it suffices to take  $\kappa^\varepsilon = \sigma_m \varepsilon^m$  for all  $m \in \mathbb{Z}$ . While it is a very interesting question to explore all the possible models, we will concentrate in this article on the relevant case for dMRI, i.e. the scaling that provides the limit model which is the best approximation of the experimental behavior, and which is  $m = 1$ . The reason is that we aim here at giving a full modeling of the dMRI process, which can be directly used by experimenters. Nevertheless, we plan to give a comprehensive presentation as well as a fully rigorous mathematical justification of all the possible limit models in another article (see [5]).

### 3 A MACROSCOPIC MODEL THROUGH TWO SCALE ASYMPTOTIC EXPANSIONS

In this section, we derive our macroscopic model through formal homogenization from the two compartment model. We note here that  $M_\varepsilon$  does not satisfy the Bloch-Torrey equation in all  $\Omega_{ext}^\varepsilon$ , but separately in  $\Omega_c^\varepsilon$  and  $\Omega_e^\varepsilon$ , with jump conditions on the  $\Gamma_m^{\varepsilon,\xi}$ 's. This remark will be important to our formal derivation of the macroscopic models.

#### 3.1 FORMAL DERIVATION OF THE MACROSCOPIC MODELS THROUGH TWO-SCALE ASYMPTOTIC EXPANSIONS

Following classical homogenization results, we are going to develop  $M_\varepsilon$  using two-scale asymptotic expansions. According to our previous remark, we are not going to introduce a unique expansion in

all  $\Omega_{\varepsilon x t}^\varepsilon$ , but two expansions, one for each phase  $\Omega_c^\varepsilon$  and  $\Omega_e^\varepsilon$ . Consequently, we write :

$$\left\{ \begin{array}{l} M_\varepsilon(\mathbf{x}, t) = M_\varepsilon^e(\mathbf{x}, t) = \sum_{i=0}^{+\infty} \varepsilon^i M_{i,e} \left( \mathbf{x}, \frac{\mathbf{x}}{\varepsilon}, t \right) \quad \text{in } \Omega_e^\varepsilon \\ M_\varepsilon(\mathbf{x}, t) = M_\varepsilon^c(\mathbf{x}, t) = \sum_{i=0}^{+\infty} \varepsilon^i M_{i,c} \left( \mathbf{x}, \frac{\mathbf{x}}{\varepsilon}, t \right) \quad \text{in } \Omega_c^\varepsilon \end{array} \right. \quad (4)$$

where the functions  $M_{i,e}(x, y, t)$  and  $M_{i,c}(x, y, t)$  are defined respectively on  $\Omega \times Y_e \times ]0, T[$  and  $\Omega \times Y_c \times ]0, T[$ , and the  $M_{i,e}(x, y, t)$  and  $M_{i,c}(x, y, t)$  are assumed  $Y$ -periodic in  $y$ . The aim of such an ansatz is to separate the "macroscopic" variations (the  $\mathbf{x}$  variable) from the "microscopic" ones (the  $y$  variable), and then try to obtain a new problem involving only the macroscopic one.

### 3.1.1 CELL EQUATIONS AND JUMP CONDITIONS

To get the equations for each of the  $M_{i,e}$ 's and the  $M_{i,c}$ 's, we start by noticing that,  $\alpha \in \{c, e\}$  :

$$\nabla M_{i,\alpha}(\mathbf{x}, \frac{\mathbf{x}}{\varepsilon}, t) = \nabla_{\mathbf{x}} M_{i,\alpha}(\mathbf{x}, \frac{\mathbf{x}}{\varepsilon}, t) + \varepsilon^{-1} \nabla_y M_{i,\alpha}(\mathbf{x}, \frac{\mathbf{x}}{\varepsilon}, t)$$

Then, we deduce :

$$\begin{aligned} \operatorname{div} \left( \sigma_\alpha \left( \frac{\mathbf{x}}{\varepsilon} \right) \nabla M_{i,\alpha}(\mathbf{x}, \frac{\mathbf{x}}{\varepsilon}, t) \right) &= \operatorname{div}_{\mathbf{x}} \left( \sigma_\alpha \left( \frac{\mathbf{x}}{\varepsilon} \right) \nabla_{\mathbf{x}} M_{i,\alpha}(\mathbf{x}, \frac{\mathbf{x}}{\varepsilon}, t) \right) + \varepsilon^{-2} \operatorname{div}_y \left( \sigma_\alpha \left( \frac{\mathbf{x}}{\varepsilon} \right) \nabla_y M_{i,\alpha}(\mathbf{x}, \frac{\mathbf{x}}{\varepsilon}, t) \right) \\ &+ \varepsilon^{-1} \operatorname{div}_{\mathbf{x}} \left( \sigma_\alpha \left( \frac{\mathbf{x}}{\varepsilon} \right) \nabla_y M_{i,\alpha}(\mathbf{x}, \frac{\mathbf{x}}{\varepsilon}, t) \right) + \varepsilon^{-1} \operatorname{div}_y \left( \sigma_\alpha \left( \frac{\mathbf{x}}{\varepsilon} \right) \nabla_{\mathbf{x}} M_{i,\alpha}(\mathbf{x}, \frac{\mathbf{x}}{\varepsilon}, t) \right) \end{aligned}$$

Now, we plug these formulae into the two compartment model, to obtain :

$$\begin{aligned} 0 &= -\varepsilon^{-2} \operatorname{div}_y (\sigma_\alpha \nabla_y M_{0,\alpha}) - \varepsilon^{-1} (\operatorname{div}_y (\sigma_\alpha (\nabla_y M_{1,\alpha} + \nabla_{\mathbf{x}} M_{0,\alpha})) + \operatorname{div}_{\mathbf{x}} (\sigma_\alpha \nabla_y M_{0,\alpha})) \\ &+ \varepsilon^0 \left( \frac{\partial M_{0,\alpha}}{\partial t} + \iota Q f(t) M_{0,\alpha} - \operatorname{div}_y (\sigma_\alpha (\nabla_y M_{2,\alpha} + \nabla_{\mathbf{x}} M_{1,\alpha})) - \operatorname{div}_{\mathbf{x}} (\sigma_\alpha (\nabla_y M_{1,\alpha} + \nabla_{\mathbf{x}} M_{0,\alpha})) \right) + \\ &\sum_{i=1}^{+\infty} \varepsilon^i \left( \frac{\partial M_{i,\alpha}}{\partial t} + \iota Q f(t) M_{i,\alpha} - \operatorname{div}_y (\sigma_\alpha (\nabla_y M_{i+2,\alpha} + \nabla_{\mathbf{x}} M_{i+1,\alpha})) - \operatorname{div}_{\mathbf{x}} (\sigma_\alpha (\nabla_y M_{i+1,\alpha} + \nabla_{\mathbf{x}} M_{i,\alpha})) \right) \end{aligned}$$

Matching each term in front of the same power of  $\varepsilon$  and expanding to all  $\mathbf{x} \in \Omega$ , we get :

$$- \operatorname{div}_y (\sigma_\alpha \nabla_y M_{0,\alpha}) = 0 \quad \text{in } \Omega \times Y_\alpha \times ]0, T[ \quad (5)$$

$$- \operatorname{div}_y (\sigma_\alpha \nabla_y M_{1,\alpha}) = \operatorname{div}_y (\sigma_\alpha \nabla_{\mathbf{x}} M_{0,\alpha}) + \operatorname{div}_{\mathbf{x}} (\sigma_\alpha \nabla_y M_{0,\alpha}) \quad \text{in } \Omega \times Y_\alpha \times ]0, T[ \quad (6)$$

$$\begin{aligned} - \operatorname{div}_y (\sigma_\alpha \nabla_y M_{2,\alpha}) &= \operatorname{div}_y (\sigma_\alpha \nabla_{\mathbf{x}} M_{1,\alpha}) - \operatorname{div}_{\mathbf{x}} (\sigma_\alpha (\nabla_y M_{1,\alpha} + \nabla_{\mathbf{x}} M_{0,\alpha})) \\ &- \frac{\partial M_{0,\alpha}}{\partial t} - \iota Q f(t) M_{0,\alpha} \end{aligned} \quad (7)$$

Next, we make the following ansatz for the jumps of  $M_\varepsilon$  and its fluxes, for  $\mathbf{x} \in \Gamma_m^\varepsilon$  :

$$[M_\varepsilon]_{|\Gamma_m^\varepsilon}(\mathbf{x}, t) = \sum_{i=0}^{\infty} \varepsilon^i \left( M_{i,e}(\mathbf{x}, \frac{\mathbf{x}}{\varepsilon}, t) - M_{i,c}(\mathbf{x}, \frac{\mathbf{x}}{\varepsilon}, t) \right) \quad (8)$$

$$[\hat{\sigma}_\varepsilon \nabla M_\varepsilon \cdot \nu]_{|\Gamma_m^\varepsilon} = \sum_{i=0}^{\infty} \varepsilon^i \left( \sigma_e \nabla M_{i,e}(\mathbf{x}, \frac{\mathbf{x}}{\varepsilon}, t) \cdot \nu - \sigma_c \nabla M_{i,c}(\mathbf{x}, \frac{\mathbf{x}}{\varepsilon}, t) \cdot \nu \right) \quad (9)$$

Then, the no-jump relation for the fluxes becomes :

$$\varepsilon^{-1} (\sigma_e \nabla_y M_{0,e} \cdot \nu - \sigma_c \nabla_y M_{0,c} \cdot \nu) + \sum_{i=0}^{\infty} \varepsilon^i (\sigma_e \nabla_y M_{i+1,e} \cdot \nu + \sigma_e \nabla_{\mathbf{x}} M_{i,e} \cdot \nu$$

$$-\sigma_c \nabla_y M_{i+1,c} \cdot \nu - \sigma_c \nabla_{\mathbf{x}} M_{i,c} \cdot \nu = 0$$

which gives, after identifying each power of  $\varepsilon$  and expanding to all  $(x, y) \in \Omega \times \Gamma_m$  :

$$\sigma_e \nabla_y M_{0,e} \cdot \nu = \sigma_c \nabla_y M_{0,c} \cdot \nu \quad \text{in } \Omega \times \Gamma_m \times ]0, T[ \quad (10)$$

and, for any  $i \geq 1$  :

$$\sigma_e \nabla_y M_{i,e} \cdot \nu + \sigma_e \nabla_{\mathbf{x}} M_{i-1,e} \cdot \nu = \sigma_c \nabla_y M_{i,c} \cdot \nu + \sigma_c \nabla_{\mathbf{x}} M_{i-1,c} \cdot \nu \quad \text{in } \Omega \times \Gamma_m \times ]0, T[ \quad (11)$$

To write the equivalent condition for the traces, recall that we have assumed that  $\kappa^\varepsilon = \varepsilon \sigma_m$ , where  $\sigma_m > 0$  is a constant independent on  $\varepsilon$ . Now we write the jump relations for traces, using (10) and (11) :

$$\begin{aligned} \sum_{i=0}^{+\infty} \varepsilon^{i+1} \sigma_m (M_{i,e} - M_{i,c}) &= \varepsilon^{-1} \sigma_\alpha \nabla_y M_{0,\alpha} \cdot \nu + \varepsilon^0 \sigma_\alpha (\nabla_y M_{1,\alpha} \cdot \nu + \nabla_{\mathbf{x}} M_{0,\alpha} \cdot \nu) \\ &+ \varepsilon^1 \sigma_\alpha (\nabla_y M_{2,\alpha} \cdot \nu + \nabla_{\mathbf{x}} M_{1,\alpha} \cdot \nu) + \sum_{i=2}^{+\infty} \varepsilon^i \sigma_\alpha (\nabla_y M_{i+1,\alpha} \cdot \nu + \nabla_{\mathbf{x}} M_{i,\alpha} \cdot \nu) \end{aligned}$$

### 3.1.2 FORMAL LIMIT PROBLEM

As usual when performing formal homogenization through two-scale asymptotic expansions, we only need (as we shall see) to obtain the equations for the first three terms,  $M_{0,\alpha}$ ,  $M_{1,\alpha}$  and  $M_{2,\alpha}$ . The problem for  $M_0$  is then given by :

$$\left\{ \begin{array}{ll} -\operatorname{div}_y(\sigma_\alpha \nabla_y M_{0,\alpha}) = 0 & \text{in } Y_\alpha \\ \sigma_\alpha \nabla_y M_{0,\alpha} \cdot \nu = 0 & \text{on } \Gamma_m \\ M_{0,e} \text{ } Y_e - \text{periodic} & \end{array} \right. \quad (12)$$

**Lemma 3.1.** *Let  $f_c \in L^2(Y_c)$ ,  $f_e \in L^2(Y_e)$ ,  $\psi_c$  and  $\psi_e \in H^{-1/2}(\Gamma_m)$ . Then, there exists a unique solution  $u_c \in H^1(Y_c)$ , up to a constant, to :*

$$\left\{ \begin{array}{ll} -\operatorname{div}_y(\sigma_c \nabla_y u_c) = f_c & \text{in } Y_c \\ \sigma_c \nabla_y u_c \cdot \nu = \psi_c & \text{on } \Gamma_m \end{array} \right.$$

if and only if, for any  $i \in \llbracket 1, N_c \rrbracket$  :

$$\int_{Y_{c,i}} f_{c+} \langle \psi_c, 1 \rangle_{H^{-1/2}(\Gamma_m \cap \partial Y_{c,i}), H^{1/2}(\Gamma_m \partial Y_{c,i})} = 0$$

and there exists a unique solution  $u_e \in H_{\sharp}^1(Y_e)$ , up to a constant, to :

$$\left\{ \begin{array}{ll} -\operatorname{div}_y(\sigma_e \nabla_y u_e) = f_e & \text{in } Y_e \\ \sigma_e \nabla_y u_e \cdot \nu = \psi_e & \text{on } \Gamma_m \\ u_e \text{ } Y_e - \text{periodic} & \end{array} \right.$$

if and only if, for any  $i \in \llbracket 1, N_e \rrbracket$  :

$$\int_{Y_{e,i}} f_{e-} \langle \psi_e, 1 \rangle_{H^{-1/2}(\Gamma_m \cap \partial Y_{e,i}), H^{1/2}(\Gamma_m \cap \partial Y_{e,i})} = 0$$

where  $H_{\sharp}^1(Y_e)$  is the space of  $H^1$  periodic functions of  $Y_e$ .

*Proof.* We detail the proof only of  $u_c$ , the proof for  $u_e$  being exactly the same. The problem for  $u_c$  gives for any  $v_c \in H^1(Y_c)$ , after using Green's formula and the Neumann boundary condition:

$$(\sigma_c \nabla_y u_c, \nabla_y v_c)_{L^2(Y_c)} = (f_c, v_c)_{L^2(Y_c)} + \langle \psi_c, \bar{v}_c \rangle_{H^{-1/2}(\Gamma_m), H^{1/2}(\Gamma_m)}$$

We introduce the scalar product on  $H^1(Y_c)$  :

$$(u_c, v_c)_{H_\sigma^1(Y_c)} = (u_c, v_c)_{L^2(Y_c)} + (\sigma_c \nabla_y u_c, \nabla_y v_c)_{L^2(Y_c)}$$

and the operator :

$$\begin{aligned} K_c : L^2(Y_c) &\longrightarrow H^1(Y_c) \\ w_c &\longmapsto K_c w_c \end{aligned}$$

where  $(K_c w_c, v_c)_{H_\sigma^1(Y_c)} = -(w_c, v_c)_{L^2(Y_c)}$  and  $F_c \in H^1(Y_c)$  is defined by

$$(F_c, v_c)_{H_\sigma^1(Y_c)} = (f_c, v_c)_{L^2(Y_c)} + \langle \psi_c, \bar{v}_c \rangle_{H^{-1/2}(\Gamma_m), H^{1/2}(\Gamma_m)}$$

Then, denoting again  $K$  the compound of  $K$  and the injection  $H^1(Y_c) \hookrightarrow L^2(Y_c)$ , which is compact according to Rellich theorem we get :

$$(I + K)u = F \quad \in L^2(Y_c)$$

which is ruled by Fredholm alternative. Consequently, we look at the kernel of  $I + K$  (as our problem is self-adjoint). If  $F = 0$ , then, for any  $v \in H^1(Y_c)$  :

$$(\sigma_c \nabla u_c, \nabla v_c)_{L^2(Y_c)} = 0$$

This implies in particular that  $u_c$  is constant in each connected component of  $Y_c$ . Thus, the compatibility condition is the orthogonality to such functions, i.e., for any  $i \in \llbracket 1, N_c \rrbracket$  :

$$\int_{Y_{c,i}} f_c + \langle \psi_c, 1 \rangle_{H^{-1/2}(\Gamma_m \cap \partial Y_{c,i}), H^{1/2}(\Gamma_m \cap \partial Y_{c,i})} = 0$$

□

The above lemma tells us that neither  $M_{0,e}$  nor  $M_{0,c}$  depend on  $y$ . The problem for  $M_1$  is consequently :

$$\begin{cases} -\operatorname{div}_y(\sigma_\alpha(\nabla_y M_{1,\alpha} + \nabla_{\mathbf{x}} M_{0,\alpha})) = 0 & \text{in } Y_\alpha \\ \sigma_e \nabla_y M_{1,e} \cdot \nu + \sigma_e \nabla_{\mathbf{x}} M_{0,e} \cdot \nu = 0 & \text{on } \Gamma_m \\ \sigma_c \nabla_y M_{1,c} \cdot \nu + \sigma_c \nabla_{\mathbf{x}} M_{0,c} \cdot \nu = 0 & \text{on } \Gamma_m \\ M_{1,e} \text{ } Y_e \text{ - periodic} \end{cases} \quad (13)$$

Thus, introducing for  $i = 1..d$  the cell problems :

$$\boxed{\begin{cases} -\operatorname{div}_y(\sigma_\alpha(\nabla_y w_{i,\alpha} + e_i)) = 0 & \text{in } Y_\alpha \\ \sigma_e \nabla_y w_{i,e} \cdot \nu + \sigma_e e_i \cdot \nu = 0 & \text{on } \Gamma_m \\ \sigma_c \nabla_y w_{i,c} \cdot \nu + \sigma_c e_i \cdot \nu = 0 & \text{on } \Gamma_m \\ w_{i,f} \text{ } Y_e \text{ - periodic} \end{cases}} \quad (14)$$

using the divergence theorem, we get :

$$\begin{aligned} \int_{Y_c} \operatorname{div}_y \sigma_c e_i &= \langle \sigma_c e_i \cdot \nu, 1 \rangle_{H^{-1/2}(\Gamma_m), H^{1/2}(\Gamma_m)} \\ \int_{Y_c} \operatorname{div}_y \sigma_e e_i &= - \langle \sigma_e e_i \cdot \nu, 1 \rangle_{H^{-1/2}(\Gamma_m), H^{1/2}(\Gamma_m)} \end{aligned} \quad (15)$$

and thus we know from lemma 3.1 that they are well-posed and consequently, and consequently we finally have :

$$M_{1,\alpha} = \sum_{i=1}^d w_{i,\alpha} \frac{\partial M_{0,\alpha}}{\partial \mathbf{x}_c} \quad \text{in } Y_\alpha \quad (16)$$

Now, we write the problem for  $M_2$  :

$$\left\{ \begin{array}{ll} -\text{div}_y(\sigma_\alpha(\nabla_y M_{2,\alpha} + \nabla_{\mathbf{x}} M_{1,\alpha})) = \text{div}_{\mathbf{x}}(\sigma_\alpha(\nabla_y M_{1,\alpha} + \nabla_{\mathbf{x}} M_{0,\alpha})) - \frac{\partial M_{0,\alpha}}{\partial t} - \iota Q f(t) M_{0,\alpha} & \text{in } Y_\alpha \\ \sigma_e \nabla_y M_{2,e} \cdot \nu + \sigma_e \nabla_{\mathbf{x}} M_{1,e} \cdot \nu = \sigma_m (M_{0,e} - M_{0,c}) & \text{on } \Gamma_m \\ \sigma_c \nabla_y M_{2,c} \cdot \nu + \sigma_c \nabla_{\mathbf{x}} M_{1,c} \cdot \nu = \sigma_m (M_{0,e} - M_{0,c}) & \text{on } \Gamma_m \\ M_{1,e} \text{ } Y_e \text{ - periodic} & \end{array} \right. \quad (17)$$

Thus, using lemma 3.1, it is easy to see that the compatibility condition for  $M_{2,e}$  implies :

$$\int_{Y_e} \text{div}_{\mathbf{x}}(\sigma_e(\nabla_y M_{1,e} + \nabla_{\mathbf{x}} M_{0,e})) - \frac{\partial M_{0,e}}{\partial t} - \iota Q f(t) M_{0,e} - \int_{\Gamma_m} \sigma_m (M_{0,e} - M_{0,i}) = 0 \quad (18)$$

while the compatibility condition for  $M_{2,c}$  implies :

$$\int_{Y_c} \text{div}_{\mathbf{x}}(\sigma_c(\nabla_y M_{1,i} + \nabla_{\mathbf{x}} M_{0,i})) - \frac{\partial M_{0,i}}{\partial t} - \iota Q f(t) M_{0,i} + \int_{\Gamma_m} \sigma_m (M_{0,e} - M_{0,i}) = 0 \quad (19)$$

The homogenized tensors  $D_c$  and  $D_e$  are defined by :

$$D_{e,ij} = \frac{1}{|Y_e|} \int_{Y_e} \sigma_e \nabla w_{j,e} \cdot e_i + \sigma_e e_j \cdot e_i \quad \text{and} \quad D_{c,ij} = \frac{1}{|Y_c|} \int_{Y_c} \sigma_c \nabla w_{j,c} \cdot e_i + \sigma_c e_j \cdot e_i$$

They can be rewritten in symmetric form :

$$\boxed{D_{\alpha,ij} = \frac{1}{|Y_\alpha|} \int_{Y_\alpha} \sigma_\alpha (\nabla w_{j,\alpha} + e_j) \cdot (\nabla w_{i,\alpha} + e_i)} \quad (20)$$

as

$$\int_{Y_\alpha} \sigma_\alpha (\nabla w_{j,\alpha} + e_j) \cdot \nabla w_{i,\alpha} = - \int_{Y_\alpha} \text{div}_y(\sigma_\alpha (\nabla w_{j,\alpha} + e_j)) w_{i,\alpha} = 0$$

as  $w_{j,\alpha}$  is solution of (14). We also introduce the two coefficients :

$$\boxed{\eta_c = \frac{\sigma_m |\Gamma_m|}{|Y_c|} \quad \text{and} \quad \eta_e = \frac{\sigma_m |\Gamma_m|}{|Y_e|}} \quad (21)$$

and then, using the fact that  $M_{0,e}$  and  $M_{0,c}$  does not depend on  $y$ , we obtain the macroscopic model:

$$\left\{ \begin{array}{ll} \frac{\partial M_{0,e}}{\partial t} + \iota Q f(t) M_{0,e} - \text{div}_{\mathbf{x}}(D_e \nabla_{\mathbf{x}} M_{0,e}) + \eta_e (M_{0,e} - M_{0,c}) = 0 & \text{in } \Omega \times ]0, T[ \\ M_{0,e}(\cdot, 0) = M_{init} & \text{in } \Omega \\ \frac{\partial M_{0,c}}{\partial t} + \iota Q f(t) M_{0,c} - \text{div}_{\mathbf{x}}(D_c \nabla_{\mathbf{x}} M_{0,c}) + \eta_c (M_{0,c} - M_{0,e}) = 0 & \text{in } \Omega \times ]0, T[ \\ M_{0,c}(\cdot, 0) = M_{init} & \text{in } \Omega \end{array} \right. \quad (22)$$

which is a coupled system of modified Bloch-Torrey equations, with a homogeneous diffusion tensor.

### 3.2 WELL POSEDNESS OF THE MACROSCOPIC MODEL

We start by giving some useful properties of the homogenized tensors.

**Lemma 3.2.** *The tensor  $D_c$  defined by (20):*

$$D_{c,ij} = \frac{1}{|Y_c|} \int_{Y_c} \sigma_c(\nabla w_{j,c} + e_j) \cdot (\nabla w_{i,c} + e_i)$$

where  $w_{i,c}$  is defined by (14) is zero, while  $D_e$  satisfies, for some  $\beta > 0$  :

$$D_e \zeta \cdot \bar{\zeta} \leq \left( \int_{Y_e} \sigma_e \right) |\zeta|^2 \quad \text{and} \quad D_e \zeta \cdot \bar{\zeta} \geq \beta \zeta \cdot \bar{\zeta}$$

*Proof.* The problem for  $w_{i,c}$  is :

$$\begin{cases} -\operatorname{div}_y \sigma_c(\nabla w_{i,c} + e_c) = 0 & \text{in } Y_c \\ \nabla_y w_{i,c} \cdot \nu + e_c \cdot \nu = 0 & \text{on } \Gamma_m \end{cases}$$

It is not difficult to check that, up to a constant (which can change in each connected component of  $Y_c$ ),  $w_{i,c} = -y_c$ , so that  $\nabla_y w_{i,c} + e_c = 0$  in  $Y_c$ . From formula (20), we deduce  $D_c = 0$ . Now, remark that :

$$D_e \zeta \cdot \bar{\zeta} = \sum_{i,j=1}^2 \int_{Y_e} \sigma_e(\nabla_y w_{j,e} \zeta_j + \zeta_j e_j) \cdot (\nabla_y w_{i,e} \bar{\zeta}_i + \bar{\zeta}_i e_i)$$

We define  $w_{\zeta,e}$  as the solution of the same problem than  $w_{j,e}$  but with  $\zeta$  instead of  $e_j$  (see the previous section for the precise definition in the five cases). By linearity, it is clear that :

$$w_{\zeta,e} = \sum_{j=1}^2 w_{j,e} \zeta_j$$

and then :

$$D_e \zeta \cdot \bar{\zeta} = \int_{Y_e} \sigma_e(\nabla_y w_{\zeta,e} + \zeta) \cdot (\nabla_y \overline{w_{\zeta,e}} + \bar{\zeta})$$

The announced upper bound is consequently obvious, as it suffices to take  $v = 0$  in the previous formula. To obtain the lower bound, we know that :

$$D_e \zeta \cdot \bar{\zeta} \geq \sigma^- \|\nabla_y w_{\zeta,e} + \zeta\|_{L^2(Y_e)}^2$$

Assume that  $\|\nabla_y w_{\zeta,e} + \zeta\|_{L^2(Y_e)}^2 = 0$ . Then, up to a constant,  $w_{\zeta,e} = -\zeta_1 y_1 - \zeta_2 y_2$ , which is incompatible with the periodicity assumption, unless  $\zeta = 0$ . Thus, for any  $\zeta \neq 0$ ,  $D\zeta \cdot \bar{\zeta} > 0$ , and  $D$  is a symmetric strictly positive tensor. To conclude, it remains to show the classical result of equivalence between coercivity and strict positivity in finite dimensional spaces. Let  $b(u, v)$  be sesquilinear form on the finite dimensional space  $V$ . Assume that :

$$b(u, v) = \overline{b(v, u)} \quad \text{and} \quad |b(u, v)| \leq C \|u\|_V \|v\|_V \quad \text{and} \quad b(u, u) > 0 \quad \forall u \neq 0$$

Consider the function :

$$F(v) = \frac{b(v, v)}{\|v\|_V^2} = b\left(\frac{v}{\|v\|_V}, \frac{v}{\|v\|_V}\right)$$

As  $V$  is of finite dimension, the unit ball is compact and thus  $F(v)$  is bounded and reaches its bound. Thus, there exists  $\beta > 0$  and  $v_{min} \in B_V(0, 1) = \{v \in V \mid \|v\|_V = 1\}$  such that :

$$\inf_{v \in B_V(0,1)} F(v) = \beta \quad \text{and} \quad F(v_{min}) = \beta$$

Consequently, by sesquilinearity, we get  $b(v, v) \geq \beta \|v\|_V^2$ , which proves that  $b$  is coercive on  $V$ ; Conversely, if  $b$  is coercive, it is obvious that it is strictly positive. Applying this to the sesquilinear form  $b(\zeta, \xi) = D\zeta \cdot \bar{\xi}$  in  $\mathbb{R}^d$ , we obtain the existence of the desired lower bound for  $D$ .

□

From this lemma, we deduce that our model simplifies in :

$$\left\{ \begin{array}{l} \frac{\partial M_{0,e}}{\partial t} + \imath Qf(t)M_{0,e} - \operatorname{div}_{\mathbf{x}}(D_e \nabla_{\mathbf{x}} M_{0,e}) + \eta_e(M_{0,e} - M_{0,c}) = 0 \quad \text{in } \Omega \times ]0, T[ \\ M_{0,e}(\cdot, 0) = M_{init} \quad \text{in } \Omega \\ \frac{\partial M_{0,c}}{\partial t} + \imath Qf(t)M_{0,i} + \eta_c(M_{0,c} - M_{0,e}) = 0 \quad \text{in } \Omega \times ]0, T[ \\ M_{0,c}(\cdot, 0) = M_{init} \quad \text{in } \Omega \end{array} \right. \quad (23)$$

Remark that the equation for  $M_{0,c}$  can be explicitly solved :

$$M_{0,c}(\mathbf{x}, t) = M_{init}G_c(\mathbf{x}, t, 0) + \int_0^t G_c(\mathbf{x}, t, s)M_{0,f}(\mathbf{x}, s)ds \quad (24)$$

where we have denoted :

$$G_c(\mathbf{x}, t, s) = \exp\left(-\int_s^t (\imath \mathbf{q} \cdot \mathbf{x}f(r) + \eta_c)dr\right) \quad (25)$$

Thus, we can decouple the system (23) :

$$\left\{ \begin{array}{l} \frac{\partial M_{0,e}}{\partial t} + (\imath Qf(t) + \eta_e)M_{0,e} - \operatorname{div}_{\mathbf{x}}(D_e \nabla_{\mathbf{x}} M_{0,f}) - \eta_e \int_0^t G_c(t, s)M_{0,e}(s)ds \\ = \eta_e M_{init}G_c(t) \quad \text{in } \Omega \times ]0, T[ \\ M_{0,e}(\cdot, 0) = M_{init} \quad \text{in } \Omega \\ M_{0,c} = M_{init}G_c(t, 0) + \int_0^t G_c(t, s)M_{0,e}(s)ds \quad \text{in } \Omega \times ]0, T[ \end{array} \right. \quad (26)$$

The first equation of (26) emphasizes the fact that this macroscopic model will behave quite differently from a Bloch-Torrey equation. In particular, the presence of the integral with respect to time will give birth to memory effects for  $M_{0,e}$ .

**Theorem 3.1.** *Let  $f \in L^\infty(0, T)$  and  $M_{init} \in L^2(\Omega) \cap L^1(\Omega)$ . We denote  $H = L^2(\Omega) \times L^2(\Omega)$ ,  $X = H^1(\Omega) \times L^2(\Omega)$  and  $X' = \tilde{H}^{-1}(\Omega) \times L^2(\Omega)$ . There exists a unique solution  $M = (M_e, M_c) \in C^0(0, T, L^2(\Omega) \cap L^1(\Omega)) \cap L^2(0, T, X)$  to the following problem :*

$$\left\{ \begin{array}{l} \frac{\partial M_e}{\partial t} + \imath Qf(t)M_e - \operatorname{div}_{\mathbf{x}}(D_e \nabla_{\mathbf{x}} M_e) + \eta_e(M_e - M_c) = 0 \quad \text{in } \Omega \times ]0, T[ \\ M_e(\cdot, 0) = M_{init} \quad \text{in } \Omega \\ \frac{\partial M_c}{\partial t} + \imath Qf(t)M_{0,i} + \eta_c(M_c - M_e) = 0 \quad \text{in } \Omega \times ]0, T[ \\ M_c(\cdot, 0) = M_{init} \quad \text{in } \Omega \end{array} \right. \quad (27)$$

which moreover satisfies :

$$\|M_e\|_{L^2(0, T, L^2(\Omega))}^2 + \|M_c\|_{L^2(0, T, L^2(\Omega))}^2 \leq \|M_{init}\|_{L^2(\Omega)}^2 \quad (28)$$

and

$$\|M_e\|_{L^2(0, T, H^1(\Omega))}^2 + \|M_c\|_{L^2(0, T, L^2(\Omega))}^2 \leq \frac{1}{\sqrt{\min(\beta, \eta_e, \eta_c)}} \|M_{init}\|_{L^2(\Omega)}^2 \quad (29)$$

where  $\beta$  is the constant of lemma 3.2.

*Proof.* It is a classical exercise of variational theory to show that solving (27) is equivalent to solve the variational formulation :

$$\begin{cases} \frac{d}{dt} \langle M(t), V \rangle_{V', V} + a_H(t; M, V) = 0 & \text{in } \mathcal{D}'(]0, T[), \quad \forall V \in X \\ M(\cdot, 0) = (M_{init}, M_{init}) & \text{in } \Omega \end{cases} \quad (30)$$

where we denote  $V = (V_e, V_c)$  any element of  $X = H^1(\Omega) \times L^2(\Omega)$ ,

$$\begin{aligned} \frac{d}{dt} \langle M(t), V \rangle_{V', V} &= \frac{d}{dt} \langle M(t), V \rangle_{\tilde{H}^{-1}(\Omega), H^1(\Omega)} + \frac{d}{dt} (M(t), V)_{L^2(\Omega)} \\ a_H(t; M, V) &= (iQf(t)M_e, V_e)_{L^2(\Omega)} + (iQf(t)M_e, V_e)_{L^2(\Omega)} + (D_e \nabla M_e, \nabla V_e)_{L^2(\Omega)} \\ &\quad + \eta_e (M_e, V_e)_{L^2(\Omega)} - \eta_e (M_c, V_e)_{L^2(\Omega)} + \eta_c (M_c, V_c)_{L^2(\Omega)} - \eta_c (M_e, V_c)_{L^2(\Omega)} \end{aligned}$$

As  $f \in L^\infty(]0, T[)$ ,  $a_H$  is measurable with respect to  $t$ , and we have, using Cauchy-Schwarz inequality and the bounds of lemma 3.2 :

$$\begin{aligned} |a(t; M, V)| &\leq \|Q\|_{L^\infty(\Omega)} \|f\|_{L^\infty} (\|M_e\|_{L^2(\Omega)} \|V_e\|_{L^2(\Omega)} + \|M_c\|_{L^2(\Omega)} \|V_c\|_{L^2(\Omega)}) \\ &\quad + \|\sigma_e\|_{L^1(Y_e)} \|\nabla M_e\|_{L^2(\Omega)} \|\nabla V_e\|_{L^2(\Omega)} + \eta_e \|M_e\|_{L^2(\Omega)} \|V_e\|_{L^2(\Omega)} + \eta_e \|M_c\|_{L^2(\Omega)} \|V_e\|_{L^2(\Omega)} \\ &\quad + \eta_c \|M_c\|_{L^2(\Omega)} \|V_c\|_{L^2(\Omega)} + \eta_c \|M_e\|_{L^2(\Omega)} \|M_c\|_{L^2(\Omega)} \end{aligned}$$

which is globally :

$$|a(t, M, V)| \leq C \|M\|_X \|V\|_X \quad \text{where} \quad \|V\|_X^2 = \|V_e\|_{H^1(\Omega)}^2 + \|V_c\|_{L^2(\Omega)}^2$$

On the other hand, we have

$$\begin{aligned} \Re a(t; M, M) &= (D_e \nabla M_e, \nabla M_e)_{L^2(\Omega)} + \eta_e (M_e, M_e)_{L^2(\Omega)} - \eta_e (M_c, M_e)_{L^2(\Omega)} \\ &\quad + \eta_c (M_c, M_c)_{L^2(\Omega)} - \eta_c (M_e, M_c)_{L^2(\Omega)} \\ &\geq \beta \|\nabla M_e\|_{L^2(\Omega)}^2 + (\eta_e - \frac{\eta_c + \eta_e}{2}) \|M_e\|_{L^2(\Omega)}^2 + (\eta_c - \frac{\eta_c + \eta_e}{2}) \|M_c\|_{L^2(\Omega)}^2 \end{aligned}$$

Thus, for any  $\lambda > \frac{\eta_c + \eta_e}{2}$ , we have :

$$\Re a(t; M, M) + \lambda \|M\|_H^2 \geq \min(\beta, \eta_e, \eta_c) \|M\|_X^2$$

Then,  $a_H$  satisfies the hypothesis of Lion's theorem (see [8]), and the result directly follows.  $\square$

We have obtain through formal homogenization a well-posed model, which is consequently suitable for modeling dMRI signals. Notice that as we have two equations in this limit model, each one corresponding to a different part of  $\Omega_{ext}^\varepsilon$ , so we have in principle :

$$M_\varepsilon \simeq M_{0,e} \quad \text{in } \Omega_e^\varepsilon \quad \text{and} \quad M_\varepsilon \simeq M_{0,c} \quad \text{in } \Omega_c^\varepsilon$$

Of course, this model can be rigorously established, and the above approximation result detailed. One can indeed prove that (see [5]) :

**Theorem 3.2.** *Under the hypothesis made on  $f$ ,  $M_{init}$ ,  $\sigma$  and  $\kappa^\varepsilon$ , we have :*

$$\begin{aligned} M_\varepsilon &\rightharpoonup \frac{|Y_e|}{|Y|} M_{0,e} + \frac{|Y_c|}{|Y|} M_{0,c} \quad \text{weakly in } L^2(0, T, L^2(\Omega)) \\ \|M_\varepsilon - M_{0,\alpha}\|_{L^\infty(0, T, L^2(\Omega_\alpha^\varepsilon))} &\rightarrow 0 \quad \text{for } \alpha \in \{c, e\} \end{aligned} \quad (31)$$

The proof is based on the periodic unfolding method, extended to the time dependent case. As it is quite a long process, and our aim here is mainly to show the efficiency of this model for dMRI experiments, this will be the object of another article (see [5]), along with the presentation and justification of the limit models for other scalings of  $\kappa^\varepsilon$ . In view of the theorem, we define :

$$M_e = \frac{|Y_e|}{|Y|} M_{0,e} \quad \text{and} \quad M_c = \frac{|Y_c|}{|Y|} M_{0,c}$$

Using (21), we have :

$$\boxed{\begin{aligned} \frac{\partial M_e}{\partial t} + \iota Q f(t) M_e - \operatorname{div}_{\mathbf{x}}(D_e \nabla_{\mathbf{x}} M_e) + \eta_e M_e - \eta_c M_c &= 0 & \text{in } \Omega \times ]0, T[ \\ M_e(\cdot, 0) &= \frac{|Y_e|}{|Y|} M_{init} & \text{in } \Omega \\ \frac{\partial M_c}{\partial t} + \iota Q f(t) M_c + \eta_c(M_c - M_e) &= 0 & \text{in } \Omega \times ]0, T[ \\ M_c(\cdot, 0) &= \frac{|Y_c|}{|Y|} M_{init} & \text{in } \Omega \end{aligned}} \quad (32)$$

it is this last model that we will use as a macroscopic model for dMRI signals.

## 4 DMRI SIGNAL MODELING

In this section, we give more details about the measured signal in a dMRI experiment and we explain how to use the model introduced in the previous section to obtain an approximation to the signal in a simple manner. In practice, the gradient magnetic field has a time profile that satisfies, at the echo time  $TE$ :

$$\int_0^{TE} f(t) dt = 0$$

and the signal is measured at  $t = TE$ . We set  $\mathbf{q} = q\mathbf{n}$ , where  $\mathbf{n}$  is a unitary vector of  $\mathbb{R}^d$ . The measured signal is given by :

$$S_\varepsilon(q, \mathbf{n}) = \int_{\mathbb{R}^d} M_\varepsilon(\mathbf{x}, TE)$$

Then, it is natural to define the approximate signal by:

$$S(q, \mathbf{n}) = \int_{\mathbb{R}^d} M(\mathbf{x}, TE)$$

where  $M = M_e + M_c$ .

### 4.1 A COUPLED ODE MODEL FOR DMRI'S SIGNALS

We denote :

$$m_{e,0} = \int_{\mathbb{R}^d} M_{e,0} \quad \text{and} \quad m_{c,0} = \int_{\mathbb{R}^d} M_{c,0} \quad \text{and} \quad m_0 = \int_{\mathbb{R}^d} M_{e,0} + M_{c,0}$$

the initial moments. These last quantities will naturally appear in the following. They are of great practical interest as :

$$\theta_e = \frac{m_{e,0}}{m_0} = \frac{|Y_e|}{|Y|} \quad \text{and} \quad \theta_c = \frac{m_{c,0}}{m_0} = \frac{|Y_c|}{|Y|}$$

represents respectively the extra-cellular volumic fraction and the intra-cellular volumic fraction, and thus contains information on the average size of the cells in the probed area. We now establish that the signal obtained from solving (32) can be equivalently obtained by solving a simpler system of coupled ODEs.

**Theorem 4.1.** *The signal obtained by solving (32) in  $L^1(0, TE, H^1(\mathbb{R}^d) \times L^2(\mathbb{R}^d)) \cap C^0(0, TE, L^2(\mathbb{R}^d) \times L^2(\mathbb{R}^d)) \cap C^0(0, TE, L^1(\mathbb{R}^d) \times L^1(\mathbb{R}^d))$  is given by :*

$$S(q, \mathbf{n}) = m(TE)$$

where  $m = m_e + m_c$ , and  $(m_e, m_c)$  is the unique solution of the system :

$$\boxed{\begin{aligned} \frac{dm_e}{dt} + q^2 \sigma_e \left( \int_0^t f(s) ds \right)^2 m_e + \eta_e m_e - \eta_c m_c &= 0 \\ \frac{dm_c}{dt} + \eta_c m_c - \eta_e m_e &= 0 \\ m_e(0) &= m_{f,0} \\ m_c(0) &= m_{c,0} \end{aligned}} \quad (33)$$

where  $\sigma_e = D_e \mathbf{n} \cdot \mathbf{n}$ .

*Proof.* Let  $(M_e, M_c)$  be the unique solution of (32) in  $C^0(0, TE, H^1(\mathbb{R}^d) \times L^2(\mathbb{R}^d)) \cap L^2(0, TE, L^2(\mathbb{R}^d) \times L^2(\mathbb{R}^d)) \cap L^2(0, TE, L^1(\mathbb{R}^d) \times L^1(\mathbb{R}^d))$ . We set :

$$\widetilde{M}_e(\mathbf{x}, t) = M_e e^{i q \mathbf{n} \cdot \mathbf{x} \int_0^t f(s) ds} \quad \text{and} \quad \widetilde{M}_c(\mathbf{x}, t) = M_c e^{i q \mathbf{n} \cdot \mathbf{x} \int_0^t f(s) ds}$$

We have, for  $\alpha \in \{c, f\}$  :

$$\frac{\partial \widetilde{M}_\alpha}{\partial t} = \left( \frac{\partial M_\alpha}{\partial t} + i U M_\alpha \right) e^{i q \mathbf{n} \cdot \mathbf{x} \int_0^t f(s) ds}$$

and :

$$\begin{aligned} \nabla \widetilde{M}_e &= \left( \nabla M_e + i q \mathbf{n} M_e \left( \int_0^t f(s) ds \right) \right) e^{i q \mathbf{n} \cdot \mathbf{x} \int_0^t f(s) ds} \\ \operatorname{div}(D_e \nabla \widetilde{M}_e) &= \left( \operatorname{div}(D_e \nabla M_e) + 2i q D_e \nabla M_e \cdot \mathbf{n} \left( \int_0^t f(s) ds \right) \right. \\ &\quad \left. - q^2 D_e \mathbf{n} \cdot \mathbf{n} \left( \int_0^t f(s) ds \right)^2 M_e \right) e^{i q \mathbf{n} \cdot \mathbf{x} \int_0^t f(s) ds} \end{aligned}$$

as  $D_e$  is symmetric. Then, as :

$$\begin{aligned} &2i q D_e \nabla M_e \cdot \mathbf{n} \left( \int_0^t f(s) ds \right) e^{i q \mathbf{n} \cdot \mathbf{x} \int_0^t f(s) ds} \\ &= 2i q D_e \nabla \widetilde{M}_e \cdot \mathbf{n} \left( \int_0^t f(s) ds \right) + 2q^2 D_e \mathbf{n} \cdot \mathbf{n} \widetilde{M}_e \left( \int_0^t f(s) ds \right)^2 \end{aligned}$$

we get :

$$\begin{aligned} \operatorname{div}(D_e \nabla \widetilde{M}_e) &= \operatorname{div}(D_e \nabla M_e) e^{i q \mathbf{n} \cdot \mathbf{x} \int_0^t f(s) ds} + 2i q D_e \nabla \widetilde{M}_e \cdot \mathbf{n} \left( \int_0^t f(s) ds \right) \\ &\quad + q^2 D_e \mathbf{n} \cdot \mathbf{n} \left( \int_0^t f(s) ds \right)^2 \widetilde{M}_e \end{aligned}$$

and then, we finally obtain the system :

$$\left\{ \begin{array}{l} \frac{\partial \widetilde{M}_e}{\partial t} - \operatorname{div}(D_e \nabla \widetilde{M}_e) + 2iqD_e \nabla \widetilde{M}_e \cdot \mathbf{n} \left( \int_0^t f(s) ds \right) + q^2 D_e \mathbf{n} \cdot \mathbf{n} \left( \int_0^t f(s) ds \right)^2 \widetilde{M}_e \\ + \eta_e \widetilde{M}_e - \eta_c \widetilde{M}_c = 0 \\ \widetilde{M}_e(\cdot, 0) = M_{e,0} \\ \frac{\partial \widetilde{M}_c}{\partial t} + \eta_c \widetilde{M}_c - \eta_e \widetilde{M}_e = 0 \\ \widetilde{M}_c(\cdot, 0) = M_{c,0} \end{array} \right. \quad \begin{array}{l} \text{in } \Omega \times ]0, TE[ \\ \text{in } \Omega \\ \text{in } \Omega \times ]0, TE[ \\ \text{in } \Omega \end{array}$$

Now, we set

$$m_e = \int_{\mathbb{R}^d} \widetilde{M}_e \quad \text{and} \quad m_c = \int_{\mathbb{R}^d} \widetilde{M}_c$$

As  $\widetilde{M}_e$  and  $\widetilde{M}_c$  both belong to  $\in C^0(0, TE, L^2(\mathbb{R}^d)) \cap L^1(\mathbb{R}^d)$ , if we denote  $\mathcal{M}_e$  and  $\mathcal{M}_c$  their fourier transform with respect to the space variable, the dual variable being denoted  $\xi$ , these transforms both belong to  $C^0([0, TE] \times \mathbb{R}^d)$  and we have :

$$m_e(t) = \mathcal{M}_e(t, 0) \quad \text{and} \quad m_c = \mathcal{M}_c(t, 0)$$

and :

$$\left\{ \begin{array}{l} \frac{\partial \mathcal{M}_e}{\partial t} + D_e \xi \cdot \xi \mathcal{M}_e - 2qD_e \xi \cdot \mathbf{n} \mathcal{M}_e \left( \int_0^t f(s) ds \right) + q^2 D_e \mathbf{n} \cdot \mathbf{n} \left( \int_0^t f(s) ds \right)^2 \mathcal{M}_e \\ + \eta_e \mathcal{M}_e - \eta_c \mathcal{M}_c = 0 \\ \frac{\partial \mathcal{M}_c}{\partial t} + \eta_c \mathcal{M}_c - \eta_e \mathcal{M}_e = 0 \end{array} \right. \quad \begin{array}{l} \text{in } \Omega \times ]0, TE[ \\ \text{in } \Omega \times ]0, TE[ \end{array}$$

We deduce from this expression that  $\mathcal{M}_e$  and  $\mathcal{M}_c$  belong to  $C^1([0, TE] \times \mathbb{R}^d)$ , and thus for  $\xi = 0$  the above expression implies directly :

$$\left\{ \begin{array}{l} \frac{dm_e}{dt} + q^2 \sigma_e \left( \int_0^t f(s) ds \right)^2 m_e + \eta_e m_e - \eta_c m_c = 0 \\ \frac{dm_c}{dt} + \eta_c m_c - \eta_e m_e = 0 \\ m_e(0) = m_{e,0} \\ m_c(0) = m_{c,0} \end{array} \right.$$

with  $\sigma_e = D_e \mathbf{n} \cdot \mathbf{n}$ . Finally, for the signal we have :

$$S = \int_{\mathbb{R}^d} M(\mathbf{x}, TE) d\mathbf{x} = \int_{\mathbb{R}^d} \widetilde{M}(\mathbf{x}, TE) e^{-iq\mathbf{n} \cdot \mathbf{x}} \int_0^T E f(s) ds d\mathbf{x} = \int_{\mathbb{R}^d} \widetilde{M}(\mathbf{x}, TE) = m(TE)$$

as  $\int_0^T E f(s) ds = 0$ , which concludes the proof.  $\square$

ODE models for the dmRI signal has appeared in the medical imaging community before [14]. However, to our knowledge, that has always been on the basis of phenomenological modeling of the experimentally obtained curves. In addition, the widely used ODE model in [14] differs from the ODE model that we describe in this paper. Our presentation seems to be the first attempt to justify ODE models from a mathematical point of view.

## 4.2 NUMERICAL EXPLORATION OF THE APPROXIMATE MODEL

In this subsection we will compare our macroscopic model to the two compartments microscopic model, with the values of the physical parameters corresponding to cerebral tissue.

The time profile of the most frequently used diffusion encoding sequence is the classic PGSE sequence which has the form:

$$f(t) = \begin{cases} 1 & 0 \leq t \leq \delta \\ 0 & \delta < t \leq \Delta \\ -1 & \Delta < t \leq \Delta + \delta \end{cases} \quad (34)$$

with  $0 \leq \delta \leq \Delta$ . By construction, we have :

$$\int_0^{\delta+\Delta} f(t)dt = 0$$

and the echo time is given by  $TE = \delta + \Delta$ .

The dMRI signal can be measured for several values of  $q$ ,  $\delta$ ,  $\Delta$  and directions  $\mathbf{n}$ . We will consequently denote  $S(q, \delta, \Delta, \mathbf{n})$  the signal (normalized by dividing by  $\int_{\mathbb{R}^d} M_{init}$ ) to emphasize this dependency. It is common in the dMRI community not to display  $S(q, \delta, \Delta, \mathbf{n})$  as a function of  $q$ , but as a function of the so called b-value :

$$b(q) = \|q\|^2 \int_0^{\Delta+\delta} \left( \int_0^t f(s)ds \right)^2 dt = \|q\|^2 \delta^2 \left( \Delta - \frac{\delta}{3} \right)$$

To understand why the quantity is used, notice that in the case of a single Bloch-Torrey equation in  $\mathbb{R}^d$  with a constant diffusion tensor  $D$  :

$$\begin{cases} \frac{\partial M}{\partial t} + iq \cdot \mathbf{x} f(t)M - \text{div}_{\mathbf{x}}(D \nabla_{\mathbf{x}} M) = 0 & \text{in } \mathbb{R}^d \times ]0, TE[ \\ M(\cdot, 0) = M_{init} & \text{in } \mathbb{R}^d \end{cases}$$

the Fourier transform  $\hat{M}$  is solution of :

$$\begin{cases} \frac{\partial \hat{M}}{\partial t} - f(t)q \cdot \nabla_{\xi} \hat{M} + \xi^T D \xi \hat{M} = 0 & \text{in } \mathbb{R}^d \times ]0, TE[ \\ \hat{M}(\cdot, 0) = \hat{M}_{init} & \text{in } \mathbb{R}^d \end{cases}$$

This problem can easily be solved using the method of characteristics, and we obtain :

$$\hat{M}(\xi, t) = \hat{M}_{init} \left( \xi + q \int_0^t f(s)ds \right) \exp \left( - \int_0^t \left( \xi + q \int_s^t f(\mu)d\mu \right)^T D \left( \xi + q \int_s^t f(\mu)d\mu \right) ds \right)$$

Then, as  $\int_{\mathbb{R}^d} M(\Delta + \delta) = \hat{M}(0, \Delta + \delta)$  we can get in this particular case an expression for the corresponding signal  $\tilde{S}$  :

$$\tilde{S}(q) = \hat{M}_{init} \left( q \int_0^{\Delta+\delta} f(s)ds \right) \exp \left( -q^T D q \int_0^{\Delta+\delta} \left( \int_s^{\Delta+\delta} f(\mu)d\mu \right)^2 ds \right)$$

As  $\int_0^{\Delta+\delta} f(s)ds = 0$ , this rewrites :

$$\tilde{S}(q) = \left( \int_{\mathbb{R}^d} M_{init} \right) \exp \left( -q^T D q \int_0^{\Delta+\delta} \left( \int_0^s f(\mu)d\mu \right)^2 ds \right)$$

and thus :

$$\tilde{S}(q) = \exp\left(-\frac{q^T D q}{\|q\|^2} b(q)\right)$$

and thus in this very particular case, the quantity  $\frac{\log S(b(q))}{b(q)}$  gives access to the coefficients of the tensor  $D$ .

In a more general setting, people who perform dMRI measure the signal, and then perform a polynomial fitting of  $\log S(b(q))$  with respect to  $b(q)$ . The coefficient of order one is called "apparent diffusion coefficient" (ADC), as in the particular situation described above it corresponds to the intrinsic diffusion tensor. The ADC is the most widely used form of imaging contrast in dMRI [15].

We now provide a few numerical results to emphasize the ability of the macroscopic model to produce a good approximation of dMRI signals when using physically realistic values for all the involved parameters. We compare of course the signal obtained using the system of ODE (33) to the signal obtained by solving the two-compartment periodic model (3).

As (3) is a problem on  $\mathbb{R}^d$ , we cannot solve it for just any initial condition. In the particular case of a constant  $M_{init}$ , it can be easily shown that the solution of (3) is quasi-periodic in space, with period  $\varepsilon$  and quasi-periodic coefficient  $\exp(-i\varepsilon q_i \int_0^t f(s) ds)$  in each direction  $e_i$ . Thus, we can solve (3) on a single periodic cell in that case, and we get the same signal (once normalized) as if we have solved it on all  $\mathbb{R}^d$ . We note that this case does not strictly enter our previous setting : indeed, such an initial condition is not  $L^1(\mathbb{R}^d)$ . However, it is easy to check that with such a  $M_{init}$ , we have :

$$M_e(\mathbf{x}, t) = m_e(t) e^{-iq \cdot \mathbf{x}} \int_0^t f(s) ds \quad \text{and} \quad M_c(\mathbf{x}, t) = m_c(t) e^{-iq \cdot \mathbf{x}} \int_0^t f(s) ds$$

where  $(M_e, M_c)$  is the solution of (32) and  $(m_e, m_c)$  the solution of (33), and thus we can still use the ODE model.

We test two situations in dimension 2, for simplicity. One is a single circular biological cell of radius  $R_m$  placed at the center of the periodic cell, for several values of  $\Delta$ , with a gradient direction  $e_x$ . The second one is the case of several circular cells of variable radii, for gradient directions  $e_x$  and  $e_y$ . We solve the ODE model (33), along with the periodic reference model (3) on a very refined mesh. Both computations are performed using `FreeFem++`[17].

A comparison of the signals obtained from the exact and approximate models is displayed on Figures 5 and 6, where the values of the other parameters are indicated. These values are chosen according to the literature in dMRI, and represent the average experimental values for the parameters usually chosen to perform realistic dMRI numerical simulations [25, 10]. We can see on these Figures that the ODE model (33) provides an excellent approximation when modeling dMRI signals for all four diffusion times  $\Delta = 5, 15, 25, 35ms$ . In particular, this approximate model accurately reproduces the 'curvature' of the signal: the obtained signals with the two models are indeed not a single exponential (the log is not a straight line), as it would be in the case of single Bloch-Torrey equation with constant coefficients (see the above computation). This phenomenon, well-known in the medical imaging community, can be reinterpreted from the ODE model : it is the fact that we have two coupled equations that induces this memory-like effect (see the end of Section 3). As both the fact that we have two equations and that they are coupled come from the scaling we have chosen for the permeability, we can thus conclude that the non-monoexponential behavior of the dMRI signal attenuation is the result of the influence of cell membranes, which acts as barriers (as our scaling corresponds to a low permeability).

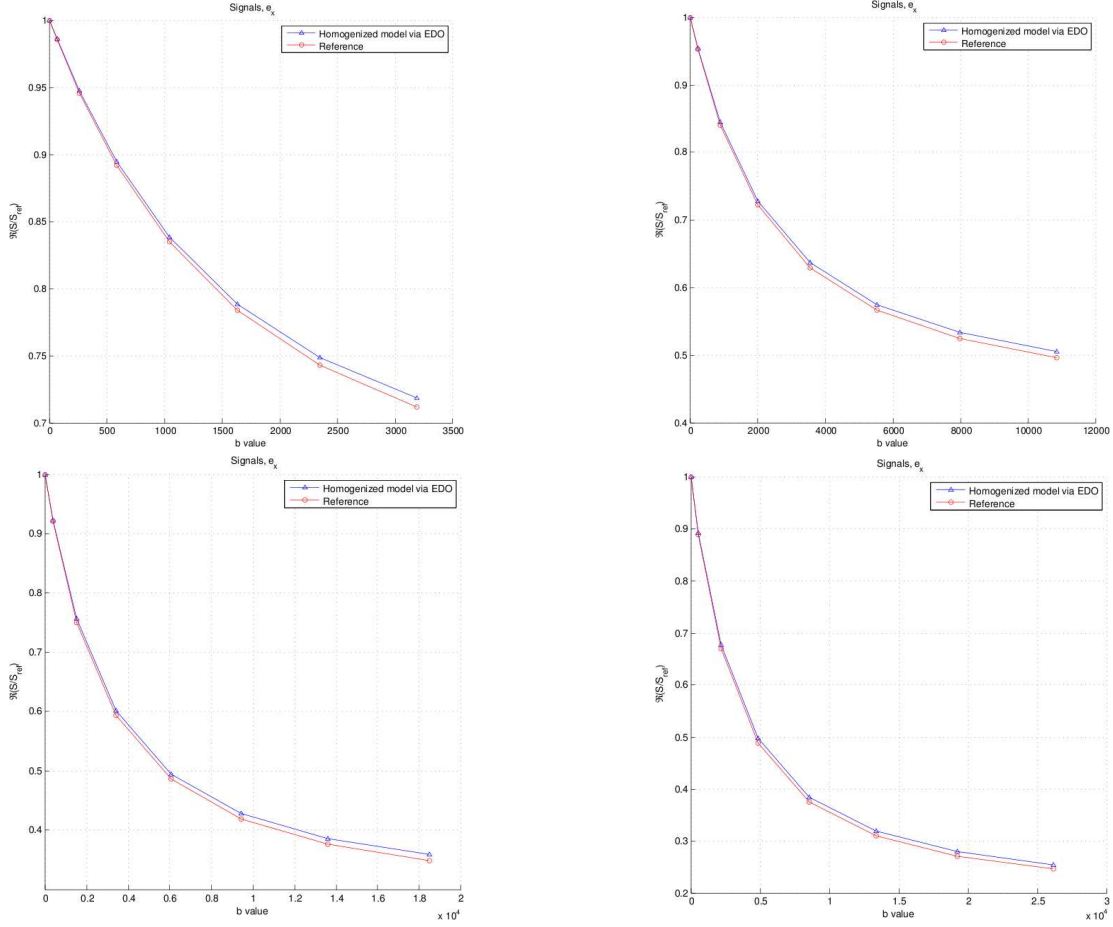


Figure 5: Normalized signals for a single circular biological cell of radius  $R_m = 0.49$  and  $\sigma_e = 3 \times 10^{-3} \text{mm}^2 \text{s}^{-1}$ ,  $\sigma_c = 1.6 \times 10^{-3} \text{mm}^2 \text{s}^{-1}$ ,  $\kappa = 15 \times 10^{-5} \text{ms}^{-1}$ ,  $\delta = 3.5 \text{ms}$ ,  $\mathbf{n} = e_x$ , for  $\Delta = 5, 15, 25$  and  $35 \text{ms}$

## 5 THE INVERSE PROBLEM : RETRIEVING MACRO PROPERTIES OF TISSUES FROM DMRI MEASUREMENTS

Now that we have checked that our model accurately reproduces the signal, the natural idea is to check whether we can retrieve the coefficients of our simplified model from the measured signals, i.e. if we can solve the inverse problem of finding the unknown coefficients  $\beta = (\eta_e, \eta_c, D_e, m_{e,0}, m_{c,0})$ . These coefficients are of great practical importance. Indeed, from initial moments, we can recover the volumic fraction, thus giving information on the concentration of cells, or their potential swelling. The coupling coefficients are also a way to obtain information on the permeability of cellular membranes, which is a very difficult quantity to measure in practice, while the homogenized tensor can give some information on the orientation of nervous fibers in the brain, for instance.

Let  $(\mathcal{S}_i)_{1 \leq i \leq N_{exp}}$  be a set of measures. For instance, we can take :

$$\mathcal{S}_i = S(q_i, \delta_i, \Delta_i \mathbf{n}_i)$$

where  $S$  is the signal from the homogenized model, or:

$$\mathcal{S}_i = S_\varepsilon(q_i, \delta_i, \Delta_i \mathbf{n}_i)$$

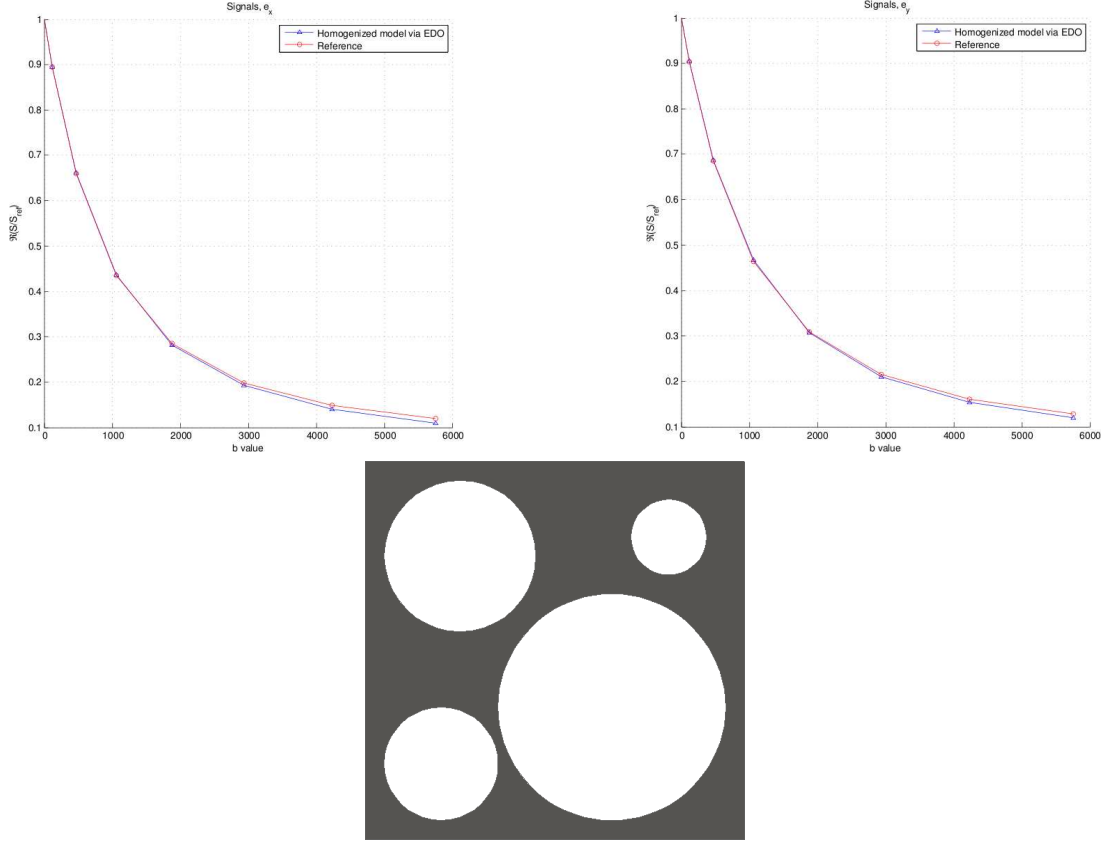


Figure 6: Normalized signals and periodic cell :  $\sigma_e = 3 \times 10^{-3} mm^2 s^{-1}$ ,  $\sigma_c = 1.6 \times 10^{-3} mm^2 s^{-1}$ ,  $\kappa = 5 \times 10^{-5} ms^{-1}$ ,  $\delta = 3.5 ms$ ,  $\Delta = 5 ms$ ,  $\mathbf{n} = e_x$  and  $e_y$

where we use measures obtained from the two compartment heterogeneous model.

As our model is only approximate, if we do not use exact data (which will of course be the case in practice), we cannot hope to find  $\beta = (\eta_e, \eta_c, D_e, m_{e,0}, m_{c,0})$  such that :

$$\mathcal{S}_i = S(q_i, \delta_i, \Delta_i \mathbf{n}_i)$$

for all  $1 \leq i \leq N_{exp}$ . This is why the natural problem is to minimize the distance between the experimental signals and the theoretical one. A natural choice is thus to solve the classical least squares problem : find  $\beta = (\eta_e, \eta_c, D_e, m_{e,0}, m_{c,0})$  which minimizes the functional :

$$G(\beta) = \sum_{i=1}^{N_{exp}} |S(q_i, \delta_i, \Delta_i \mathbf{n}_i) - \mathcal{S}_i|^2$$

This least squares problem can be tackled numerically using one of the many methods of the literature for solving inverse problems using least squares. As our purpose here is to illustrate the feasibility of this inverse problem, we have chosen to use a the well tested interior-reflective Newton method described in [7] and [6] and implemented in `Matlab` under the name `lsqnonlin`. To generate the measures, we have used the parameters :

$$\sigma_e = 3 \times 10^{-3} mm^2 s^{-1}, \quad \sigma_c = 1.6 \times 10^{-3} mm^2 s^{-1}, \quad \kappa = 5 \times 10^{-5} ms^{-1}$$

and computed the signals from models (33) and (3) for directions  $e_x$  and  $e_y$ , for  $q_i = 0.000015 * i$ ,  $i = 0..25$ , and for  $(\delta, \Delta) = (3.5, 5), (3.25, 7.5), (3, 10), (2.75, 12.5) ms$ . We now provide results for the

two situations described in the previous section.

First, we consider the case of a single circular biological cell of radius  $R_m = 0.49$ . To solve our minimization problem, we use a random starting set of parameters  $\beta_0$  that are at most 50% different in the  $l^\infty$  norm from the exact set of parameters  $\beta^*$  we are looking for. We provide results for several values of  $\beta_0$  on Table 1 (we display  $(\eta_e, \eta_c, \theta_c, D_e(0, 0), D_e(0, 1), D_e(1, 0), D_e(1, 1))$  in each entry of the table, as it is equivalent in our case to known  $\theta_c$  and  $m_0 = S(0, \delta_i, \Delta_i, \mathbf{n}_i)$  or  $m_{e,0}$  and  $m_{c,0}$ ).

<i>Type of data</i>	<i>Initial guess</i>	<i>Homogenization</i>	<i>Inversion</i>
<i>Non-homogenized signal <math>\mathcal{S}_\varepsilon</math></i>	0.00072825	0.00062439	0.00083039
	0.00021223	0.00020424	0.00024101
	0.9028	0.75352	0.87943
	0.0011	0.00090387	0.0011329
	$2.2630e - 09$	$3.3371e - 09$	$2.263e - 09$
	$2.0958e - 09$	$3.3371e - 09$	$2.0958e - 09$
	0.0014	0.00090397	0.0011329
<i>Non-homogenized signal <math>\mathcal{S}_\varepsilon</math></i>	0.00041904	0.00062439	0.0004921
	0.00010878	0.00020424	0.0002121
	0.7996	0.75352	0.7187
	0.0012	0.00090387	0.00083655
	$3.9017e - 09$	$3.3371e - 09$	$3.9017e - 09$
	$2.3041e - 09$	$3.3371e - 09$	$2.3041e - 09$
	0.00078547	0.00090397	0.00083658
<i>Homogenized signal <math>\mathcal{S}</math></i>	0.00075905	0.00062439	0.00067182
	0.00024167	0.00020424	0.00020651
	0.7882	0.75352	0.75021
	0.00073191	0.00090387	0.00094546
	$2.8164e - 09$	$3.3371e - 09$	$2.8164e - 09$
	$4.1110e - 09$	$3.3371e - 09$	$4.111e - 09$
	0.00064833	0.00090397	0.00094556
<i>Homogenized signal <math>\mathcal{S}</math></i>	0.00062060	0.00062439	0.00088715
	0.00016355	0.00020424	0.00022292
	0.9699	0.75352	0.90318
	0.0010	0.00090387	0.0011188
	$3.3381e - 09$	$3.3371e - 09$	$3.3381e - 09$
	$3.2792e - 09$	$3.3371e - 09$	$3.2792e - 09$
	0.00066511	0.00090397	0.0011189

Table 1: Numerical inversion for the case of a single circular biological cell, for two randomly chosen initial sets  $\beta_0$

We see from these results that, as can be expected, the estimated parameters are closer to the real, homogenized values, when we use the signals from model (33) than when we use the non-homogenized signal coming from model (3). Indeed, the modeling error, corresponding to the fact that (33) is an approximation of (3) and thus the signals coming from these two models, while being close, are not equal, can be reinterpreted as the fact that (3) provides "noisy" data when we try to solve the inverse problem for (33).

It can also be observed on Table 1 that the quality of the estimated coefficients seems to depend on our initial guess. To limit the effect of this arbitrary choice, we have solved the inverse problem for several initial guesses, and took the values of the estimated coefficients that correspond to the smallest residual. Results are displayed on Table 2. We see on Table 2 that the results are in this case more robust, and that we obtained a quite good approximation of our homogenized coefficients.

<i>Type of data</i>	<i>Initial guesses</i>	<i>Homogenization</i>	<i>Inversion</i>
<i>Non-homogenized signal <math>\mathcal{S}_\varepsilon</math></i>	10	0.00062439	0.00084568
		0.00020424	0.00023061
		0.75352	0.60243
		0.00090399	0.0011663
		$7.3873e - 09$	$7.2782e - 09$
		$7.3873e - 09$	$1.0272e - 08$
<i>Non-homogenized signal <math>\mathcal{S}_\varepsilon</math></i>	15	0.00062439	0.00064367
		0.00020424	0.00022337
		0.75352	0.68816
		0.00090399	0.00097322
		$7.3873e - 09$	$7.8142e - 09$
		$7.3873e - 09$	$6.0091e - 09$
<i>Non-homogenized signal <math>\mathcal{S}_\varepsilon</math></i>	20	0.00062439	0.00063403
		0.00020424	0.0002231
		0.75352	0.6957
		0.00090399	0.00096379
		$7.3873e - 09$	$6.8829e - 09$
		$7.3873e - 09$	$1.1063e - 08$
<i>Homogenized signal <math>\mathcal{S}</math></i>	10	0.00062439	0.00081316
		0.00020424	0.00022011
		0.75352	0.95444
		0.00090399	0.001063
		$7.3873e - 09$	$7.3733e - 09$
		$7.3873e - 09$	$1.0349e - 08$
<i>Homogenized signal <math>\mathcal{S}</math></i>	15	0.00062439	0.00062805
		0.00020424	0.00020354
		0.75352	0.73866
		0.00090399	0.0009066
		$7.3873e - 09$	$9.3574e - 09$
		$7.3873e - 09$	$9.9634e - 09$
		0.00090393	0.00090654

Table 2: Numerical inversion for the case of a single circular biological cell, using several initial sets  $\beta_0$

To further improve the results, one could wonder if we could use some of the link between the parameters. In particular, notice that we have:

$$\frac{\eta_e}{\eta_c} = \frac{\theta_c}{\theta_e} = \frac{\theta_c}{1 - \theta_c} \quad \text{and} \quad m_{c,0} = \theta_c m_0$$

and consequently :

$$m_{c,0} = \frac{\eta_e m_0}{\eta_e + \eta_c}$$

Thus, we can eliminate  $m_{c,0}$  in our inversion process. We reproduce the above study in this case. We display on Table 3 the inversion from one randomly chosen set of initial guesses, while on Table 4 we again display the values of the estimated parameters that correspond to the smallest residual from

<i>Type of data</i>	<i>Initial guess</i>	<i>Homogenization</i>	<i>Inversion</i>
<i>Non-homogenized signal <math>\mathcal{S}_\varepsilon</math></i>	0.00059987	0.00062439	0.00056023
	0.00030261	0.00020424	0.00021833
		0.75352	0.71957
	0.00059331	0.00090387	0.00089672
	$4.5236e - 09$	$3.3371e - 09$	$4.5236e - 09$
	$3.8202e - 09$	$3.3371e - 09$	$3.8202e - 09$
	0.00079212	0.00090397	0.00089675
<i>Non-homogenized signal <math>\mathcal{S}_\varepsilon</math></i>	0.00043140	0.00062439	0.0005243
	0.00018959	0.00020424	0.00021462
		0.75352	0.70955
	0.00088762	0.00090387	0.00086532
	$2.0711e - 09$	$3.3371e - 09$	$2.0711e - 09$
	$3.6358e - 09$	$3.3371e - 09$	$3.6358e - 09$
	0.00065645	0.00090397	0.00086535
<i>Homogenized signal <math>\mathcal{S}</math></i>	0.00073690	0.00062439	0.00069693
	0.00019858	0.00020424	0.00020925
		0.75352	0.76908
	0.00086721	0.00090387	0.00096295
	$3.9885e - 09$	$3.3371e - 09$	$3.9885e - 09$
	$2.5031e - 09$	$3.3371e - 09$	$2.5031e - 09$
	0.00070501	0.00090397	0.00096305
<i>Homogenized signal <math>\mathcal{S}</math></i>	0.00032186	0.00062439	0.00055099
	0.00030310	0.00020424	0.00019789
		0.75352	0.73575
	0.00060304	0.00090387	0.00084013
	$2.0230e - 09$	$3.3371e - 09$	$2.023e - 09$
	$2.9113e - 09$	$3.3371e - 09$	$2.9113e - 09$
	0.00063108	0.00090397	0.00084022

Table 3: Numerical inversion for the case of a single circular biological cell, for two randomly chosen initial sets  $\beta_0$ , using the constraint  $\theta_c = \frac{\eta_e}{\eta_e + \eta_c}$

several randomly chosen initial guesses. We see on these two Tables that the estimated parameters are much closer to the exact homogenized values when we use this constraint, even when using a single randomly chosen initial guess (the results being of course still better when we perform several estimations). Thus, it seems that adding this constraint can improve parameter estimation through solving the inverse problem.

Finally, we display on Table 5 the results obtained for the periodic cell of Figure 6, where there are 4 circular cells of different sizes, with the parameters :

$$\sigma_e = 3 \times 10^{-3} mm^2 s^{-1}, \quad \sigma_c = 1.6 \times 10^{-3} mm^2 s^{-1}, \quad \kappa = 5 \times 10^{-5} m s^{-1}$$

and measures obtained for the same input parameters,  $q$ ,  $\mathbf{n}$ ,  $\delta$ ,  $\Delta$ , as before. We use the constraint and perform several initial guesses, taking again the parameters corresponding to the smallest residual. We see that even in this more complicated situation, the inverse problem still gives good estimates of the parameters.

<i>Type of data</i>	<i>Initial guesses</i>	<i>Homogenization</i>	<i>Inversion</i>
<i>Non-homogenized signal <math>\mathcal{S}_\varepsilon</math></i>	10	0.00062439	0.00055388
		0.00020424	0.00021904
		0.75352	0.7166
		0.00090399	0.00088566
		$7.3873e - 09$	$8.128e - 09$
		$7.3873e - 09$	$4.9688e - 09$
		0.00090393	0.00088551
<i>Homogenized signal <math>\mathcal{S}</math></i>	10	0.00062439	0.00058975
		0.00020424	0.00020164
		0.75352	0.74521
		0.00090399	0.00087136
		$7.3873e - 09$	$1.035e - 08$
		$7.3873e - 09$	$1.0633e - 08$
		0.00090393	0.0008713

Table 4: Numerical inversion for the case of a single circular biological cell, using several initial sets  $\beta_0$ , under the constraint  $\theta_c = \frac{\eta_e}{\eta_e + \eta_c}$

<i>Type of data</i>	<i>Initial guesses</i>	<i>Homogenization</i>	<i>Inversion</i>
<i>Non-homogenized signal <math>\mathcal{S}_\varepsilon</math></i>	10	0.00047981	0.00032008
		0.00046232	0.00038455
		0.50928	0.45425
		0.001948	0.0017607
		$7.7789e - 06$	$8.1847e - 06$
		$7.7789e - 06$	$4.1457e - 06$
		0.0017534	0.0015911
<i>Homogenized signal <math>\mathcal{S}</math></i>	10	0.00047981	0.00045812
		0.00046232	0.00045389
		0.50928	0.50232
		0.001948	0.0019139
		$7.7789e - 06$	$9.5453e - 06$
		$7.7789e - 06$	$6.6441e - 06$
		0.0017534	0.0017228

Table 5: Numerical inversion for the case of the periodic cell of Figure 6, using several initial sets  $\beta_0$ , under the constraint  $\theta_c = \frac{\eta_e}{\eta_e + \eta_c}$

## 6 CONCLUSION

We have proposed a new macroscopic model for the signal obtained from dMRI experiments. This new model, obtained through homogenization of the two-compartment Bloch-Torrey equation, accurately reproduces the memory effects commonly observed experimentally, and explains it as the influence of cellular membranes on the diffusion of water. This model is a good candidate for obtaining in practice quantitative macroscopic information on the probed tissue through solving the inverse problem on the ODE model. The complete mathematical justification of the homogenization process as well as the study of the uniqueness of the solution of the inverse problem will be the subject of another article.

## REFERENCES

- [1] R. ANDREW AND B. MACVICAR. *Imaging cell volume changes and neuronal excitation in the hippocampal slice*. Neuroscience, vol. 62, pp. 371-383, 1994.
- [2] T. ARBOGAST. *Gravitational forces in dual-porosity systems: I. model derivation by homogenization*. Transport in Porous Media, volume 13: pp. 179–203, 1993.
- [3] T. ARBOGAST. *Gravitational forces in dual-porosity systems: Ii. computational validation of the homogenized model*. Transport in Porous Media, volume 13: pp. 205–220, 1993.
- [4] D. L. BUCKLEY, J. D. BUI, M. I. PHILLIPS, AND S. J. BLACKBAND. *Mri measurement of cell volume fraction in the perfused rat hippocampal slice*. Magn. Reson. Med., vol. 42, no. 3, pp. 603-607, 1999.
- [5] J. COATLÉVEN. *Mathematical justification of macroscopic models for diffusion mri through the periodic unfolding method*. Preprint, 2012.
- [6] T. COLEMAN AND Y. LI. *On the convergence of reflective newton methods for large-scale nonlinear minimization subject to bounds*. Mathematical Programming, Vol. 67, Number 2, pp. 189-224, 1994.
- [7] T. COLEMAN AND Y. LI. *An interior, trust region approach for nonlinear minimization subject to bounds*. SIAM Journal on Optimization, Vol. 6, pp. 418-445, 1996.
- [8] R. DAUTRAY AND J.-L. LIONS. *Mathematical analysis and numerical methods for science and technology, volume 5 : evolution problems*. Springer, 1993.
- [9] J. FLINT, B. HANSEN, P. VESTERGAARD-POULSEN, AND S. J. BLACKBAND. *Diffusion weighted magnetic resonance imaging of neuronal activity in the hippocampal slice model*. NeuroImage, vol. 46, pp. 411-418, 2009.
- [10] K. D. HARKINS, J.-P. GALONS, T. W. SECOMB, AND T. P. TROUARD. *Assessment of the effects of cellular tissue properties on adc measurements by numerical simulation of water diffusion*. Magn. Reson. Med., volume 62 (6): pp. 1414–1422, 2009. ISSN 1522-2594. URL <http://dx.doi.org/10.1002/mrm.22155>.
- [11] Y. HASEGAWA, M. FISHER, L. L. LATOUR, B. J. DARDZINSKI, AND C. H. SOTAK. *Mri diffusion mapping of reversible and irreversible ischemic injury in focal brain ischemia*. Neurology, vol. 44, no. 8, p. 1484, 1994.
- [12] Y. HASEGAWA, M. FISHER, L. L. LATOUR, B. J. DARDZINSKI, AND C. H. SOTAK. *Mri diffusion mapping of reversible and irreversible ischemic injury in focal brain ischemia*. Neurology, vol. 44, no. 8, p. 1484, 1994.
- [13] M. A. HORSFIELD AND D. K. JONES. *Applications of diffusion-weighted and diffusion tensor mri to white matter diseases : a review*. NMR Biomed., vol. 15, no. 7-8, pp. 570-577, 2002.
- [14] J. KARGER, H. PFEIFER, AND W. HEINIK. *Principles and application of self-diffusion measurements by nuclear magnetic resonance*. Advances in magnetic resonance, volume 12: pp. 1–89, 1988.
- [15] D. LEBIHAN AND H. JOHANSEN-BERG. *Diffusion mri at 25: Exploring brain tissue structure and function*. NeuroImage, no. 0 pp.
- [16] D. LEBIHAN, S. I. URAYAMA, T. ASO, T. HANAKAWA, AND H. FUKUYAMA. *Direct and fast detection of neuronal activation in the human brain with diffusion mri*. PNAS, vol. 103, no. 21, pp. 8263-8268, 2006.

- [17] O. PIRONNEAU, F. HECHT, AND J. MORICE. *freefem++*, [www.freefem.org/](http://www.freefem.org/).
- [18] W. S. PRICE. *Pulsed-field gradient nuclear magnetic resonance as a tool for studying translational diffusion: Part 1. basic theory*. Concepts Magn. Reson., volume 9 (5): pp. 299–336, 1997. ISSN 1099-0534. URL [http://dx.doi.org/10.1002/\(SICI\)1099-0534\(1997\)9:5<299::AID-CMR2>3.0.CO;2-U](http://dx.doi.org/10.1002/(SICI)1099-0534(1997)9:5<299::AID-CMR2>3.0.CO;2-U).
- [19] D. SCHNAPAUFF, M. ZEILE, M. B. NIEDERHAGEN, B. FLEIGE, P.-U. TUNN, B. HAMM, AND O. DUDECK. *Diffusion-weighted echo-planar magnetic resonance imaging for the assessment of tumor cellularity in patients with soft-tissue sarcomas*. J. Magn. Reson. Imaging, vol. 29, no. 6, pp. 1355-1359, 2009.
- [20] E. O. STEJSKAL AND J. E. TANNER. *Spin diffusion measurements: Spin echoes in the presence of a time-dependent field gradient*. The Journal of Chemical Physics, volume 42 (1): pp. 288–292, 1965. URL <http://dx.doi.org/10.1063/1.1695690>.
- [21] T. SUGAHARA, Y. KOROGI, M. KOCHI, I. IKUSHIMA, Y. SHIGEMATU, T. HIRAI, T. OKUDA, L. LIANG, Y. GE, Y. KOMOHARA, Y. USHIO, , AND M. TAKAHASHI. *Usefulness of diffusion-weighted mri with echo-planar technique in the evaluation of cellularity in gliomas*. J. Magn. Reson. Imaging, vol. 9, no. 1, pp. 53-60, 1999.
- [22] H. TORREY. *Bloch equations with diffusion terms*. Physical Review Online Archive (Prola), volume 104 (3): pp. 563–565, 1956. URL <http://dx.doi.org/10.1103/PhysRev.104.563>.
- [23] Y. TSUSHIMA, A. TAKAHASHI-TAKETOMI, AND K. ENDO. *Magnetic resonance (mr) differential diagnosis of breast tumors using apparent diffusion coefficient (adc) on 1.5-t*. J. Magn. Reson. Imaging, vol. 30, no. 2, pp. 249-255, 2009.
- [24] S. WARACH, D. CHIEN, M. R. W. LI, AND R. R. EDELMAN. *Fast magnetic resonance diffusion-weighted imaging of acute human stroke*. Neurology, vol. 42, no. 9, pp. 1717-, 1992.
- [25] J. XU, M. DOES, AND J. GORE. *Numerical study of water diffusion in biological tissues using an improved finite difference method*. Physics in medicine and biology, volume 52 (7): pp. –, 2007. ISSN 0031-9155. URL <http://view.ncbi.nlm.nih.gov/pubmed/17374905>.